Article

Coupling of Advanced Oxidation Technologies and Biochar for the Removal of Dyes in Water

Carolina Gallego-Ramírez [1] ![ORCID], Edwin Chica [1] ![ORCID] and Ainhoa Rubio-Clemente [1,2,*] ![ORCID]

[1] Grupo de Investigación Energía Alternativa (GEA), Facultad de Ingeniería, Universidad de Antioquia UdeA, Calle 70 No 52-21, Medellín 050010, Colombia
[2] Escuela Ambiental, Facultad de Ingeniería, Universidad de Antioquia UdeA, Calle 70 No 52-21, Medellín 050010, Colombia
* Correspondence: ainhoa.rubioc@udea.edu.co

Abstract: When dyes are discharged in water bodies, mutagenic, carcinogenic and teratogenic effects may be caused in both aquatic organisms and human beings. The use of biochar and the implementation of advanced oxidation processes (AOPs) are alternative treatments that have been used individually in the removal of dyes in wastewater. Besides being effective processes acting separately, biochar and AOPs can be coupled, exhibiting synergetic effects in the treatment of dyes contained in water. This work deals with the methods implemented to produce biochar from biomass, its mechanism in the removal of dyes and associated sustainability issues. Additionally, the main AOPs that have been utilized for the removal of dyes from water are covered, as well as the biochar-AOP combined processes. The future prospects for the removal of dyes from water have been also addressed. The coupling of biochar to AOPs has been proven to be more effective in the removal and mineralization of dyes than the individual treatments. In this regard and considering the scarce studies in the field, new horizons are opened on the treatment of water polluted with dyes.

Keywords: advanced oxidation process; biochar; dye; sustainability; synergetic effect

1. Introduction

Water pollution requires instant and realistic solutions [1]. A wide range of industrial activities generates and discards high volumes of wastewater into the environment, causing the pollution of water bodies [2]. The massive use of dyes around the word has caused the presence of these substances in water [3]. When dyes are discharged into the environment, they end up in rivers, lakes and other water bodies, resulting in negative impacts in the aquatic ecosystem [4]. About 20,000 tons of textile dyes are released into water due to an inefficient dyeing process [5]. From 17 to 20% of polluted water comes from the textile industry [6]. Dyes can affect water transparency even at concentrations of 0.1 mg/L [7]. Coloration of water bodies interferes with light diffusion, altering photosynthetic processes and, due to dye toxicity and recalcitrance potential, they become a hazard for aquatic life and public health [8].

Conventional physicochemical and biological treatments, like coagulation–flocculation, biological treatments, electrochemical reduction and membrane filtration, have been used to eliminate dyes in wastewater. However, these methods have some disadvantages, including low efficiency when dyes are present at low levels, sludge production and high operational costs [9,10]. In this regard, biochar has been regarded as a promising adsorbing material to treat water polluted with dyes, due to its low cost and sustainability [11]. As reported in the literature, biochar can remove up to 98% of the dye contained in water [12,13]. In the same way, advanced oxidation processes (AOPs) represent another alternative treatment to treat dyes in water. The main chemical species involved in the high efficiency of AOPs for the removal of dyes in the aquatic matrix is the hydroxyl radical ($^\bullet$OH). Additionally, sulfate radicals ($SO_4^{\bullet-}$) can play a major role in the degradation of these pollutants [14]. In the

elimination of dyes, AOPs have been shown to be an effective treatment, since efficiencies up to 98% have been achieved [15].

Biochar and AOPs not only represent a potential removal of dyes as individual treatments, but there is also evidence suggesting that the combination of these two treatments might have a synergetic effect [16,17]. When biochar is used as a catalyst in AOPs, it can increase the generation of $^\bullet OH$ and $SO_4^{\bullet-}$ [18]. Biochar ability as activator of hydrogen peroxide (H_2O_2) and persulfate (S_2O_8) is due to the presence of oxygen-containing groups and environmentally persistent radicals on its surface [19,20]. Biochar can be synthetized with metal ions, metal oxides or metal composites, so that the role of biochar as a catalyst is increased, making it suitable to be used along with AOPs, such as Fenton and photocatalysis [8]. When used together (biochar plus AOPs), dyes are not only removed in water, but they are degraded to less harmful compounds and even mineralized. In this regard, biochar-AOP combined treatment can efficiently decrease the negative impacts associated with wastewater containing dyes [21]. Furthermore, the regeneration ability of biochar gives it the option to be used in several cycles of reaction without reducing its efficiency, making the biochar a cost effective and sustainable heterogeneous adsorbing material and catalyst, with application in industrial wastewater treatment due to its low production and operational costs [22,23].

Under this scenario, the objective of this work is to provide evidence that biochar and AOPs can be coupled and used as a highly efficient treatment for the removal and mineralization of dyes contained in water. In this regard, the thermochemical methods for biochar generation are covered, as well as the biochar mechanism for the elimination of dyes and its regeneration ability. Similarly, this work describes the most important AOPs that have been used for the treatment of dyes in water. Finally, the role of biochar in the implementation of AOPs for the treatment of dyes, its advantages, feasible transformation and mechanisms for the activation of H_2O_2 and S_2O_8 are discussed.

2. Materials and Methods

The Scopus database was used to select scientific works that had been published up to the year 2021. This database was used since it is regarded as the largest database in the world. Therefore, it is considered as one of the most suitable to carry out this kind of studies in the area of interest [24]. In Scopus, an initial search was conducted for scientific articles dealing with the removal of dyes in wastewater by using biochar, AOPs and processes in which both types of treatments were combined.

Three different search strings were carried out. In the first one, the keywords [TITLE-ABS-KEY ("biochar" AND "wastewater")] were used, and for the second and the third ones, the search criteria [TITLE-ABS-KEY ("advanced" AND "oxidation" AND "processes" AND "wastewater")] and [TITLE-ABS-KEY ("biochar" AND "advanced" AND "oxidation" AND "process")] were used. For the first search, 2054 results were obtained from 2009, which represents the year in which the first publications were reported, until 2021 (Figure 1). The second search string yielded 5644 results, ranging from the year in which the first publication was reported (1970) to 2021 (Figure 2). In turn, 138 documents were found in the third search stage, which were reported from 2012 to 2021 (Figure 3).
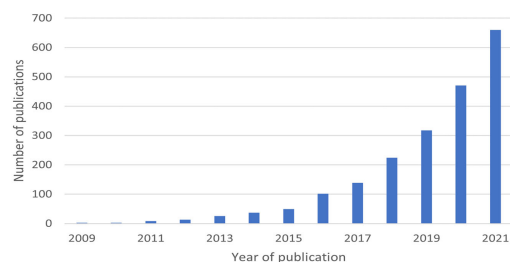

Figure 1. Documents published from 2009 to 2021 under the search criterion [TITLE-ABS-KEY ("biochar" AND "wastewater")].
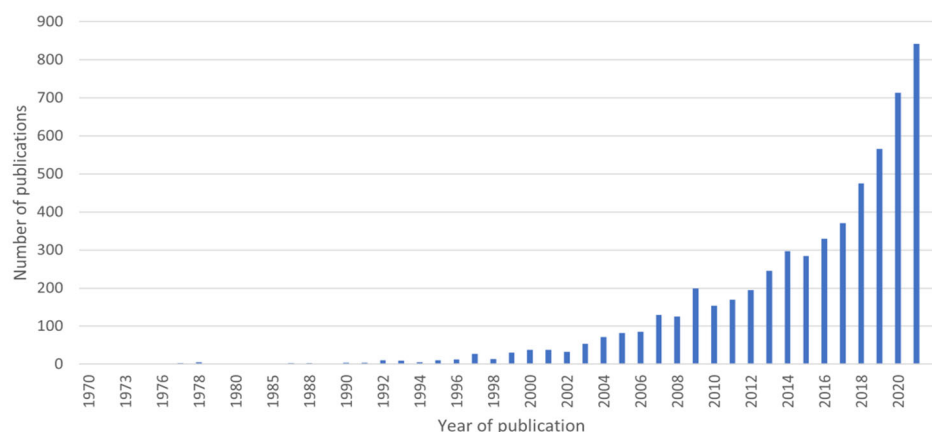
Figure 2. Documents published from 1970 to 2021 under the search criterion [TITLE-ABS-KEY ("advanced" AND "oxidation" AND "processes" AND "wastewater")].
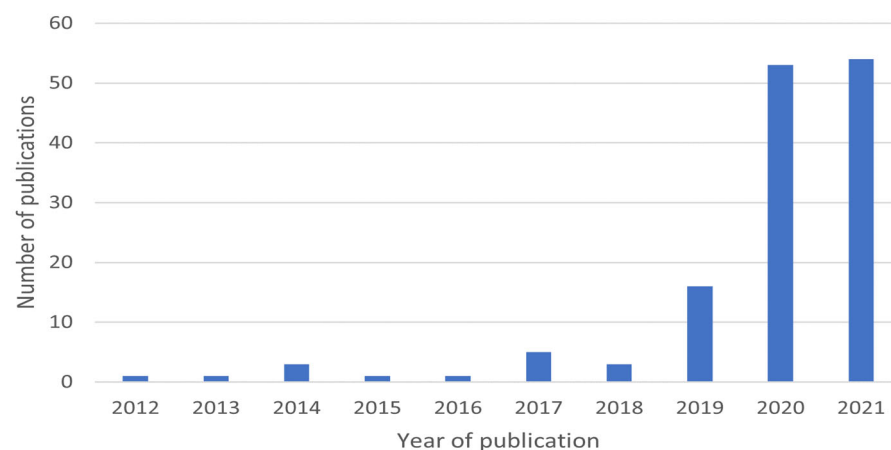
Figure 3. Documents published from 2012 to 2021 under the search criterion [TITLE-ABS-KEY ("biochar" AND "advanced" AND "oxidation" AND "process")].

The central theme of the current work is the coupling of biochar and AOPs for the removal of dyes in wastewater. Therefore, the documents found from the search string related to the keywords [TITLE-ABS-KEY ("biochar" AND "advanced" AND "oxidation" AND "process")] were further analyzed. In Figure 4, the results were compiled and classified depending on the type of document.

Figure 4. Publications classified according to the type of document.

Since the Scopus database is continuously updated, it is important to note that the results illustrated here could change when the same search criteria are used again. Addi-

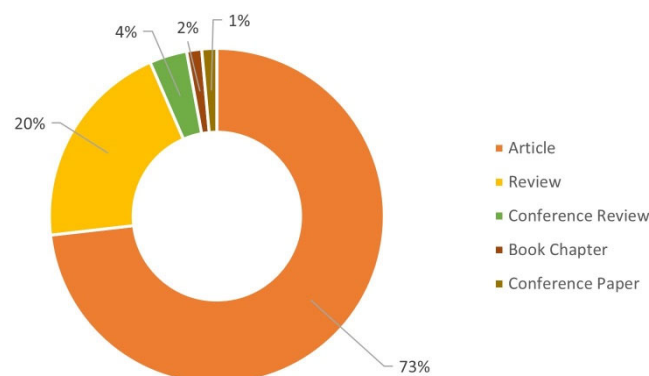tionally, the results for both the number of publications and publications per year, by type of document and by country will be different from those presented here when the search strings are modified.

3. Results

Using the first search string ([TITLE-ABS-KEY ("biochar" AND "wastewater")]), 2054 results were obtained, with China being the country with the highest number of publications, followed by the United States and India. Although the largest number of publications was found in China, the predominant language was English, with 94.7% of publications written in this language. Moreover, 84% of the publications found under the first criterion were scientific articles, 9.4% were review articles, and 6.6% were divided between conference papers, book chapters, conference reviews, errata, article data, editorials, short notes and surveys.

In Figure 1, a growth in the number of publications is observed, with 2020 and 2021 being the years with the highest number of publications (471 and 660, respectively). Concerning the second search (5644 results), China was again observed to be the country with the highest number of publications, followed this time by the United States and Spain. English was also the predominant language (~94%), as expected, followed by Mandarin (~4%); the rest of the publications were written in Spanish, Portuguese and French, among other languages. Under this search criterion, research and review articles represented the two most reported types of documents (75% and 11.6%, respectively). In turn, Figure 2 shows that the publications related to the use of AOPs in wastewater treatment have an ascending distribution from 1970 to 2021. This growth is constant from 2016 up to present. 2021 was thus the year with the highest number of publications, since 842 publications were reported.

In turn, in the last search stage, which includes the main issue of the current work (i.e., the coupling of biochar and AOP in the removal of dyes in wastewater), 135 documents of the total of results obtained (138 works) were published in English, with the remaining 3 being written in Mandarin. Figure 3 illustrates the rise in the number of publications alluding to this main topic from 2012 to 2021, the latter being the year with the highest number of publications (54). Figure 4 shows that the types of documents into which the publications are divided are research articles, review articles, conference reviews, book chapters and conference articles. Research articles comprised the majority of publications, with a percentage of 73.2%. This fact suggests that there is an interest within the scientific community in the experimental development of processes in which biochar and advanced oxidation technologies are combined. In turn, the country with the highest number of publications was China (94). This might be because China is the largest textile producer in the world and is making efforts to fill the gaps in its legislation concerning wastewater including dyes [24,25]. China was followed by the United States (19) and Australia (14). Furthermore, in Latin America, the country with the highest number of publications was Brazil (2), followed by Colombia and Argentina with one publication each. In the United States, there has been a growing interest in the evaluation of the recovery of resources based on wastewater. This may explain its growing interest in the development of wastewater treatments [26]. In the case of Australia, which stands out as the third country with the highest number of publications on the subject of biochar coupled with AOPs, there is restrictive legislation regarding wastewater discharges, in which maximum allowable values for the discharge of wastewater with the presence of dyes are presented [27]. Therefore, the need to implement effective treatments in the removal of dyes reflects the interest in the development of new technologies worldwide [18].

From the results obtained in this research, a growing concern in the use of biochar and AOPs in the treatment of wastewater is observed. Likewise, an increasing interest in the integration of both treatments is found. Indeed, the application of biochar in the removal of dyes is observed to be focused on the use of modified biochar, which in turn, can be

coupled with AOPs, achieving high efficiencies in the removal and mineralization of the dyes contained in water.

4. Discussion

4.1. Removal of Dyes by Biochar

4.1.1. Production of Biochar

Biochar is a carbon-rich by-product produced from the thermal decomposition of biomass. Biomass used to produce biochar can come from different sources; any organic material, agro-industrial waste, animal manure, microalgae, sewage sludge, wood and agricultural waste are some of the biomass sources reported in literature [18]. It is important to note that the biomass used in the production of biochar is usually a waste; this helps with the management of waste and contributes to sustainable development [28]. Biochar is produced via pyrolysis, hydrothermal carbonization, gasification, and torrefaction [29].

Pyrolysis is conducted in an oxygen free atmosphere [30]. Pyrolysis can be divided into slow pyrolysis, fast pyrolysis, flash carbonation and microwave-assisted pyrolysis. The differences between these types of pyrolysis are the heating rate, residence time and the heating method [31]. In slow pyrolysis, the biomass is decomposed at temperatures between 450 and 500 °C, with a heating range of 0.1 and 1 °C/s, and a residence time from 5 to 30 min. During the process, nitrogen gas is used to avoid oxygen presence. Slow pyrolysis is beneficial because biochar is produced in a higher amount in comparison with the liquid and the gaseous products [30,32]. In turn, fast pyrolysis is done under high temperatures, normally ranging from 850 to 1250 °C, with a heating range of 60 °C/min and a short residence time from 0.5 to 1 s. In fast pyrolysis, the production of biochar yield is less, and bio-oil is produced in a higher amount compared to that generated in a slow process [33]. Gezahegn et al. [34] showed that biochar from fast pyrolysis has higher concentrations of phytotoxic volatile fatty acids like acetic and pentanoic acids than biochar derived from slow pyrolysis, suggesting that extending residence times in pyrolysis can lead to a biochar free of toxic effects. Flash carbonation is conducted under temperatures ranging from 800 to 1200 °C, with a retention time less than 0.5 s and a heating range of more than 1000 °C/min; this process requires high pressures, usually higher than 1 MPa, and produces high amounts of biochar [31,35,36]. In turn, microwave-assisted pyrolysis is a process where biomass is heated by energetic radiation emitted from a microwave source; this method provides a quick start up and ending of the heating process, and a higher heating rate [36].

On the other hand, hydrothermal carbonization is carried out at temperatures ranging from 180 to 300 °C in the presence of water and with a pressure above the water saturation pressure to prevent water evaporation [37]. In hydrothermal carbonization, the product is often known as hydrochar [38]. The process of gasification is carried out under high temperatures, from 600 to 900 °C, and an oxidative atmosphere with the presence of gasifying agents like air, steam, oxygen, carbon dioxide (CO_2) or a mixture of these gases [39]. The amount of biochar yield from gasification is generally less than the one formed in pyrolysis because of the partial oxidation conditions in which some carbon is converted into carbon monoxide (CO) [40]. It is important to note that biochar produced from gasification of biomass can contain high levels of alkali and alkaline metals, as well as polycyclic aromatic hydrocarbons (PAHs) [41]. In torrefaction, biomass is decomposed in an inert atmosphere with temperatures ranging from 200 to 300 °C at a slow heating rate [42]. During torrefaction, the biomass chemical structures are destroyed, causing a significant removal of oxygen [43]. Moreover, in torrefaction, hydroxyl groups are removed from biochar, leading to the production of hydrophobic groups [44].

4.1.2. Dye Removal by Adsorption Using Biochar

Biochar adsorption efficacy depends on the method and biomass used for its production. The biochar surface area, pore structure and functional groups are affected by the temperature used in the decomposition of biomass [45]; i.e., an increase in the temperature

produces a biochar with a higher grade of carbonization, aromaticity, surface area, stability, ash content and basic pH [46]. Some features of biochar improving its adsorption capacity of pollutants are its high surface area, well-developed pore structure, high carbon content, oxygenated functional groups and high cation exchange capacity [47]. The adsorption mechanism of biochar includes electrostatic attraction, pore filling, π-π interactions, hydrophobic interactions, and H-bonding phenomena [48]. The oxygenated functional groups, such as hydroxyl, carboxyl and ketone groups, present in the biochar surface are one of the main active adsorption sites for dyes; these oxygenated compounds help with surface complexation, H-bonding and electrostatic attraction. These functional groups also have been found to contribute to dye removal by electron-transfer reactions [49]. It is reported that biochar obtained from hydrothermal carbonization could contain more oxygenated functional groups and, unlike pH and the surface area, an increase in the temperature used in the decomposition of the biochar can reduce the abundance and diversity of the oxygenated functional groups on biochar surface [50,51]. The aromatic structure of biochar helps with dye adsorption. When biochar is produced at high temperatures, a large content of π-electrons is generated, favoring interactions π-π and, subsequently, increasing dye adsorption [52]. Biochar surface is usually high on hydroxyl ions (OH$-$); therefore, biochar has a negatively charged surface that favors electrostatic attraction of positively charged dyes molecules [53]. Biochar surface area and pore structure also increase biochar physical adsorption capacity [48]. In Table 1, several studies where biochar has been used in the elimination of dyes are compiled.

Table 1. Dye removal by adsorption using biochar.

Biomass	Thermal Decomposition Method	Dye	Optimal Operation Conditions	Removal Efficiency	Adsorption Mechanism	Ref.
Chrysanthemum morifolium Ramat straw	Hydrothermal carbonization 220 °C	Basic red 46	pH = 10; [Biochar] = 0.03 g; t = 120 min	53.19 mg/g	Electrostatic attraction and H-bonding-π-π interaction	[54]
Chromolaena odorata	Slow pyrolysis 800 °C for 3 h	Indigo carmine	[Biochar] = 30 mg T = 30 °C; t = 2 h	98.8 mg/g	Physical adsorption and electrostatic attraction	[55]
Pinus patula wood	Gasification 700 °C, atmospheric air as gasification agent	Malachite green	pH =10; [Biochar] = 9.80 g/L; Biochar particle size =150–300 μm; t = 60 min; [dye] = 50 mg/L	>99.70%	Not specified	[56]
Date palm petioles	Slow pyrolysis 700 °C, 3 h of retention time	Crystal violet	pH = 7; T = 30 °C	209 mg/g	Electrostatic attraction, pore-filling, H-bonding and π-π interaction	[13]
Groundnut shell	Slow pyrolysis 350 °C during 120 min	Basic red 09	pH = 8; [Biochar] = 1 g/L; T = 35 °C	46.3 mg/g	Ion exchange	[57]

Dye adsorption on biochar can be affected by the solution pH, biochar dosage and temperature [58]. The pH of the solution can affect the adsorbate (in this case, the dye) and the adsorbent (biochar). Depending on the pH, the dye can change its characteristics and properties; likewise, the solution pH can impact biochar surface charge and the availability of its functional groups [52]. Adsorbate and adsorbent have functional groups that can be protonated or deprotonated, resulting in the production of different surface charges. These surface charges depend on the solution pH and promote electrostatic attraction or repulsion between the dye and the biochar [59]. Biochar dosage can have

mixed effects on dye adsorption. Sometimes when the biochar dosage is increased, binding sites increase too, enhancing dye adsorption; however, in other cases, the increase in biochar dosage can lead to biochar particles binding together, reducing the adsorption capacity [54,58]. Furthermore, the adsorption capacity can reach a stable level, so that regardless the biochar dosage increase, the adsorption efficiency stays constant at a certain value [60]. Temperature, as mentioned above, affects the adsorption capacity too, since an increase in temperature decreases the viscosity of the solution, augmenting the dye mobility and promoting intraparticle diffusion to the pores on the biochar surface [52]. Nevertheless, an increase in temperature can have a negative effect on dye adsorption; when adsorption is exothermic, there is a weak adsorption force between the active sites of biochar and the dye molecule, resulting in a decrease in dye adsorption. Hence, the strength of the adsorption force depends on whether the adsorption process is endothermic or exothermic [52,61]. Thus, the optimization of these parameters is of the utmost importance [62].

4.1.3. Biochar Regeneration and Final Disposal

The regeneration and reusability capacity of biochar can prolong its life, make it useful in practical applications, reduce operation costs and help with sustainable development [63,64]. Biochar can be used in various cycles of adsorption-desorption and with the proper regeneration method, the efficiency of dye removal can show a minimal decline [58,65].

Thermal and chemical regeneration are two of the methods used for biochar regeneration [52]. Thermal regeneration consists of the degradation of the adsorbate (i.e., dyes in this case) present on biochar surface by applying heat. In turn, in chemical regeneration, a solvent is used to achieve the removal or the decomposition of the dye present on the biochar surface. In this method, the chemical agent used is usually an acid, a base or a hot solvent. It may be highlighted that the aforementioned method is effective whether the concentration of the dye is low [36]. Literature reports on the chemical regeneration of biochar include the use of compounds such as methanol (CH_3OH), acetic acid (CH_3COOH), sodium hydroxide (NaOH), acetone (C_3H_6O), benzene (C_6H_6), ethanol (C_2H_5OH) and hydrochloric acid (HCl) as solvents, while for thermal regeneration, an activation of the used biochar at 850 °C has been observed [36,65–69]. When the removal efficiency of the regenerated biochar decreases considerably, and it is not possible or appealing to use the biochar for another adsorption-desorption cycle, biochar should be disposed so that secondary pollution is avoided [65,69]. For the disposal of the biochar used, several methods have been reported, including incineration for energy recovery, landfill disposal, bio-oil and fertilizer production, and soil amendment [70,71]. It should be noted that for some of these methods, dye molecules should not only be adsorbed on the biochar surface, but they must be also degraded, since dyes can leach from the biochar surface, causing secondary pollution [72]. Efforts must be made to find the safest disposal method for the biochar that contains dyes, to reduce this secondary risk.
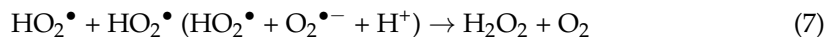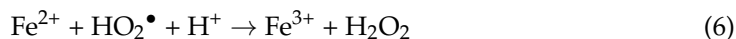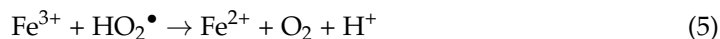
4.2. Dye removal by Advanced Oxidation Processes

AOPs are a group of physicochemical (ozonation, Fenton, peroxonation, sono-chemical cavitation, UV/H_2O_2, UV/O_3, UV/TiO_2, UV/ZnO) and electrochemical (electrooxidation, electro-Fenton) processes where the generation of oxidants such as $OH^\bullet$ helps degrade pollutants [73]. AOPs are known as highly efficient processes to treat wastewater due to their high mineralization efficiency and rapid oxidation reaction rate [74]. AOPs are based on the production of the non-selective $OH^\bullet$; however, depending on the process, other reactive oxygen species (ROS) can be generated such as $SO_4^{\bullet-}$, hydroperoxyl radicals ($HO_2^\bullet$) and superoxide radicals ($O_2^{\bullet-}$), which can degrade pollutants in water [75]. The ROS generated in AOPs can react with the pollutants in three different ways: (i) hydrogen abstraction, (ii) hydroxylation addition and (iii) electron transfer [73]. When AOPs are used to treat wastewater that have inorganic ions such as chlorides (Cl^-), carbonates (CO_3^{2-}), bicarbonates (HCO_3^-), and phosphates (PO_4^{3-}), those inorganic ions can act as scavengers and introduce different types of reactive species that have a lower oxidant power.

Therefore, the removal efficiency of the process decreases [76]. For the removal of dyes, the application of AOPs, e.g., Fenton, UV/H_2O_2, sono-photocatalysis and persulfate-AOP, has been reported [74,77–79].

4.2.1. Fenton Process

The Fenton reaction consists of the degradation of H_2O_2 by ferrous or ferric ions (Fe^{2+} and Fe^{3+}, respectively); even though Fe^{3+} ions are more abundant and cost less than the Fe^{2+} ions, the formation of $^\bullet OH$ is higher by using Fe^{2+} ions [80]. The Fenton process occurs through the formation of radicals; all the reaction set represented by Equations (1)–(7) occurs simultaneously. Along with the reactions expressed in Equation (1), the recycling of Fe^{3+} ions to Fe^{2+} ions shown in reaction (5) plays an important role in the Fenton process and can be the rate-determining step of the catalytic cycle [81]. The high oxidizing power of $^\bullet OH$ can completely mineralize complex and non-biodegradable organic substances such as dyes [82]. The Fenton reaction like other AOPs could be affected by the presence of Cl^-, CO_3^{2-}, HCO_3^-, PO_4^{3-}, NO_3^-, NO_2^- and SO_4^{2-} ions, as these compounds can act as $^\bullet OH$ scavengers, decreasing the removal efficiency [83].

$$Fe^{2+} + H_2O_2 \rightarrow Fe^{3+} + {}^\bullet OH + OH^- \tag{1}$$

$$Fe^{3+} + H_2O_2 \rightarrow Fe^{2+} + HO_2^\bullet + H^+ \tag{2}$$

$${}^\bullet OH + H_2O_2 \rightarrow HO_2^\bullet + H_2O \tag{3}$$

$${}^\bullet OH + Fe^{2+} \rightarrow Fe^{3+} + OH^- \tag{4}$$

$$Fe^{3+} + HO_2^\bullet \rightarrow Fe^{2+} + O_2 + H^+ \tag{5}$$

$$Fe^{2+} + HO_2^\bullet + H^+ \rightarrow Fe^{3+} + H_2O_2 \tag{6}$$

$$HO_2^\bullet + HO_2^\bullet \ (HO_2^\bullet + O_2^{\bullet-} + H^+) \rightarrow H_2O_2 + O_2 \tag{7}$$
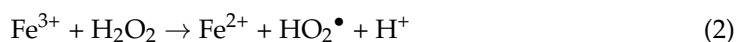
In the Fenton process, the concentration of H_2O_2 needs to be optimized to favor the maximum generation of $^\bullet OH$, since when a concentration above the optimum of H_2O_2 is used in the process, the rates of the reactions on Equations (2)–(7) are increased, leading to a consumption of $^\bullet OH$ and the generation of other radicals like $HO_2^\bullet$ that have a lower oxidation potential. Therefore, the removal efficiency of the Fenton process is decreased. Moreover, when H_2O_2 is used in a high concentration, the chemical oxygen demand (COD) of the treated water can increase [84,85].

Parameters including pH, temperature and Fe concentration must be optimized [80]. The importance of the solution pH is that at low pH values, H^+ ions become a stronger scavenger of $^\bullet OH$. Additionally, with a higher concentration of H^+ ions, H_2O_2 tends to be stabilized as hydroxyoxidanium ($H_3O_2^+$), resulting in the inhibition of Fe^{2+} regeneration. On the other hand, at a high pH, Fe^{3+} ions tend to be hydrolyzed and precipitate, decreasing the catalytic capacity of the Fe^{3+} ions. In fact, it has been shown that the optimum range of pH in the Fenton process is from 2 to 4 pH units [85,86]. An increase in temperature can cause a positive and negative effect. On the positive side, an increase in the system temperature increases the reaction rate; however, temperature can facilitate the decomposition of H_2O_2 [80]. When the iron concentration is not optimized, an excess of Fe^{2+} ions increases the level of suspended solids within the solution, as well as the conductivity of the water, leading to the formation of sludge containing iron [85].

To overcome the limitations of the conventional Fenton process, the heterogeneous Fenton process, photo-Fenton process, sono-Fenton process, and electro-Fenton process have been developed [86]. Nevertheless, all these processes have associated disadvantages.

Heterogeneous Fenton Process

In a heterogeneous Fenton process, solids containing insoluble iron such as iron oxide (Fe_2O_3), magnetite (Fe_3O_4) and iron (III) oxide-hydroxide (FeOOH) or iron supported on a solid like clay, carbon material, zeolite and polymer are used as suppliers of Fe^{2+} ions [87].

In this type of process, the catalytic Fenton reaction occurs on the surfaces of the solid catalyst. This helps prevent the leaching of iron, extends the operational pH range including the usual wastewater pH (2–9) and reduces the concentration of iron in the formed sludge. Additionally, the use of a solid catalyst leads to an easy separation, regeneration, and reuse of the catalyst [84,86]. In a heterogeneous Fenton process, there is a possibility that the iron leaches from the catalyst surface, meaning that the catalyst and H_2O_2 are going to react and produce $^\bullet OH$ by the homogeneous Fenton reaction (Equation (1)) as well as by heterogeneous Fenton reactions [88]. The decomposition of H_2O_2 by means of heterogeneous catalysts is described by Equations (8)–(11). In these equations, iron is in the form of iron oxide present in goethite, and $\equiv Fe^{III}$ is the iron present in the goethite surface [89].

$$\equiv Fe^{III} - OH + H_2O_2 \rightarrow (H_2O_2)s \tag{8}$$

$$(H_2O_2)s \rightarrow (\equiv FeII\bullet O_2H) + H_2O \tag{9}$$

$$(\equiv Fe^{II\bullet} O_2H) \rightarrow \equiv Fe^{II} + HO_2^\bullet \tag{10}$$

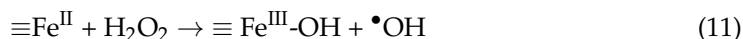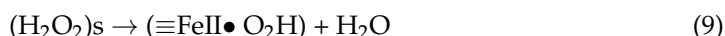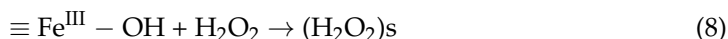$$\equiv Fe^{II} + H_2O_2 \rightarrow \equiv Fe^{III}\text{-}OH + {}^\bullet OH \tag{11}$$

Photo-Fenton Process

The conventional Fenton process cannot lead to a complete mineralization [83]. Therefore, to achieve this purpose and increase the effectiveness in the Fenton process, the conventional Fenton process is assisted by sunlight or ultraviolet light (UV) at a wavelength ranging from 290 to 400 nm. Light enhances the photolysis of H_2O_2 and promotes the formation of Fe^{2+} ions by the reduction of Fe^{3+} ions [83]. The pathways of production of Fe^{2+} ions and the photolysis of H_2O_2 are shown in Equations (12) and (13) [90]. Since photo-Fenton process has the same problem with the solution pH as the conventional Fenton, heterogeneous photo-Fenton processes have been investigated, with the design of the right solid catalyst being the major challenge [91].

$$Fe^{3+} + H_2O + hv \rightarrow Fe^{2+} + {}^\bullet OH + H^+ \tag{12}$$

$$H_2O_2 + hv \rightarrow 2{}^\bullet OH \tag{13}$$

Electro-Fenton Process

The electro-Fenton process merges conventional Fenton and electrochemical technology. In electro-Fenton the generation of H_2O_2 is in situ. The main reactions in the electro-Fenton process are presented in Equations (14) and (15) [92]. As shown in Equation (14), H_2O_2 is generated by two electron-oxygen reduction reactions and will react with Fe^{2+} ions, producing $^\bullet OH$ (Equation (15)). Similarly to other Fenton-related processes, electro-Fenton can be homogeneous or heterogeneous [93].

$$O_2 + 2H^+ + 2e^- \rightarrow H_2O_2 \tag{14}$$

$$Fe^{2+} + H_2O_2 \rightarrow Fe^{3+} + {}^\bullet OH + OH^- \tag{15}$$

As described above, an advantage of the electro-Fenton process is the generation of H_2O_2. This helps avoid the transportation of H_2O_2; however, the electro-Fenton process has another three types of operation [94]: (i) H_2O_2 is added to the solution from the outside, and the source of Fe^{2+} ions is a sacrificial iron anode (Equation (16)); (ii) Fe^{2+} ions are electrogenerated with a sacrificial iron anode (Equation (16)) and H_2O_2 by an oxygen-sparging cathode (Equation (17)); and (iii) H_2O_2 and Fe^{2+} ions are added to the solution externally and $^\bullet OH$ are produced in an electrolytic cell and in the cathode, Fe^{3+} ions are reduced to Fe^{2+} ions (Equation (18)) [80]. Other advantages of the electro-Fenton process are the production of less iron sludge than conventional Fenton, and that the reactants used

in the process are economic and have low toxicity. Additionally, the process operation is simpler in terms of control when compared to the conventional Fenton [95].

$$Fe \rightarrow Fe^{2+} + 2e^- \tag{16}$$

$$O_2 + 2H^+ + 2e^- \rightarrow H_2O_2 \tag{17}$$

$$Fe^{3+} + e^- \rightarrow Fe^{2+} \tag{18}$$

Sono-Fenton Process

When ultrasound is applied to water, the acoustic cavitation phenomenon is produced. This results from the application of sound waves with a frequency ranging from 20 to 1000 kHz by means of an ultrasound generator [96]. Cavitation generates microbubbles in the water that collapse, generating an adiabatic heating of the vapor that is inside the bubble [97]. This creates hot spots with temperatures above 5000 °C and ultrahigh pressure above 2000 atm. The energy that this process liberates can pyrolyze water molecules, resulting in the formation of hydrogen radicals ($^\bullet$H), $^\bullet$OH and HO$_2{}^\bullet$, as well as H_2O_2, as described by Equations (19)–(23) [97,98]. In these equations,))) represents ultrasonic irradiation.

$$H_2O +))) \rightarrow H^\bullet + {}^\bullet OH \tag{19}$$

$$O_2 +))) \rightarrow 2O^\bullet \tag{20}$$

$$H_2O + O^\bullet \rightarrow 2{}^\bullet OH \tag{21}$$

$$O_2 + H^\bullet \rightarrow O^\bullet + {}^\bullet OH \tag{22}$$

$$2{}^\bullet OH \rightarrow H_2O_2 \tag{23}$$

When ultrasound is combined with the Fenton process, a higher amount of $^\bullet$OH is produced. The combination of the processes causes mixing of the solution. This results in an improvement in the contact between $^\bullet$OH and pollutants (dyes in this case), an enhancement regeneration of Fe^{2+} ions, a reduction in the production of sludge and an improvement of the clean and reactive surface of the solid catalyst; the latter occurs when ultrasound is coupled with heterogeneous Fenton specifically [99,100].
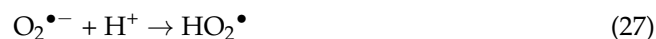
4.2.2. UV/H$_2$O$_2$ System

When UV irradiation is combined with H_2O_2, two $^\bullet$OH are formed, as shown in Equation (13) [101]. The UV/H$_2$O$_2$ process has several advantages, like no sludge production and efficient removal of COD in a brief period of reaction time [102]. In this process, parameters like the solution pH, ultraviolet (UV) lamp and temperature must be optimized; i.e., the concentration of H_2O_2 must be optimized as covered previously, due to its ability to scavenge $^\bullet$OH. In terms of the solution pH, this process performs better when the pH solution is in the range from 3 to 5. Low or medium pressure UV lamps (LP-UV or MP-UV) can be used, with the MP-UV lamps being better due to their ability to irradiate large spectrum waves faster than LP-UV lamps. Concerning the solution temperature, an increase can lead to a higher amount of $^\bullet$OH, but a temperature above the optimum decomposes H_2O_2 into water and oxygen [102].
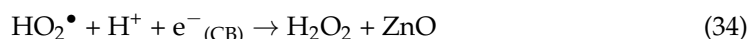
4.2.3. Photocatalysis and Sono-photocatalysis

Sono-photocatalysis is a treatment where a catalyst is irradiated by UV light and at the same time ultrasonic waves are applied to the solution [103]. In the literature, the use of titanium dioxide (TiO$_2$) and zinc oxide (ZnO) is reported as the main catalysts to be used in these treatments of dyes in water [104]. The combination of photolysis, sonolysis and catalyst results in the generation of electron-hole pairs at an elevated temperature and pressure (due to cavitation) and, therefore, $^\bullet$OH are formed (Equations (24)–(29)). $^\bullet$OH also are formed during the sonolysis of water molecules. This increases the level of the $^\bullet$OH, resulting in the total mineralization of pollutants [105]. When in sono-photocatalysis

the catalyst used is a heterogeneous one, an increase in the rate of formation of cavitation microbubbles occurs, increasing the lysis of water molecules and, subsequently, the generation of $^\bullet OH$ [106]. Furthermore, heterogenous cavitation can release the molecules of the pollutants or by-products that are blocking the surface of the catalyst, increasing the UV available sites and eliminating the mass transfer limitation that can occur during the process [107].
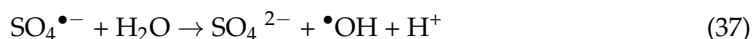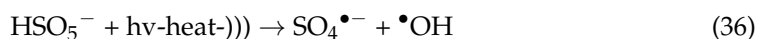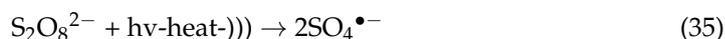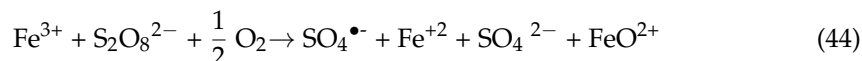
$$TiO_2 + hv \rightarrow TiO_2 \ (e^- + h^+) \tag{24}$$

$$h^+{}_{(VB)} + OH- \ ads \rightarrow {}^\bullet OH \tag{25}$$

$$e^-{}_{(CB)} + O_2 \rightarrow O_2{}^{\bullet -} \tag{26}$$

$$O_2{}^{\bullet -} + H^+ \rightarrow HO_2{}^\bullet \tag{27}$$

$$2 \ HO_2{}^\bullet \rightarrow H_2O_2 + O_2 \tag{28}$$

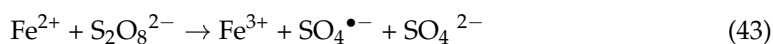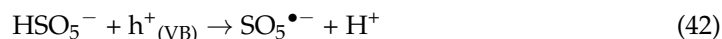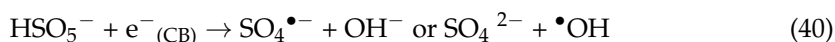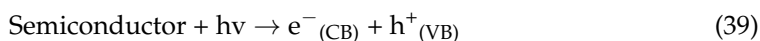$$H_2O_2 + hv \rightarrow 2{}^\bullet OH \tag{29}$$

Even though TiO_2 has been widely used as a catalyst in AOPs, it can generate toxic effects on the environment. Leite et al. [108] studied the ecotoxicity of TiO_2 in its rutile form in *Mytilus galloprovincialis* (known as Mediterranean mussel). When mussels were exposed to TiO_2, damage to mussel gills was reported in a dose-dependent manner. Additionally, the mussels showed an increase in the content of lipofuscin in the central vessel, indicating that TiO_2 generates oxidative stress in the mussels. Unlike TiO_2, ZnO is not toxic to the environment and living organisms; and it is cheaper, therefore, it can be applied for a large-scale water treatment [109]. It is important to note that the ZnO mechanism is similar to that for TiO_2 in sono-photocatalysis processes (Equations (30)–(34)).

$$ZnO + hv \rightarrow ZnO \ (e^- + h^+) \tag{30}$$

$$h^+{}_{(VB)} + OH- \ ads \rightarrow {}^\bullet OH \tag{31}$$

$$e^-{}_{(CB)} + O2 \rightarrow O_2{}^{\bullet -} \tag{32}$$

$$O_2{}^{\bullet -} + H^+ \rightarrow HO_2{}^\bullet \tag{33}$$

$$HO_2{}^\bullet + H^+ + e^-{}_{(CB)} \rightarrow H_2O_2 + ZnO \tag{34}$$

4.2.4. Persulfate-Based AOPs

Persulfate-based AOPs have gained attention for the degradation of organic pollutants such as dyes due to the advantages that $SO_4{}^{-\bullet}$ have over $^\bullet OH$, including longer half-life, stronger oxidation potential, diverse activation methods of persulfate and easy storage and transportation. Additionally, persulfate-based AOPs are less dependent on the operating conditions than H_2O_2-based AOPs [51,110,111]. Persulfate (SO^{2-}), peroxymonosulfate (PMS, $HSO_5{}^-$) and peroxydisulfate (PDS/PS, $S_2O_8{}^{2-}$) can be activated to generate $SO_4{}^{-\bullet}$ by thermal, UV and ultrasonic energy, catalysis (homogeneous and heterogeneous), transition metals and carbonaceous materials [110]. As shown in Equations (30)–(33), when PDS/PS (Equation (35)) and PMS (Equation (36)) are photolyzed, sonolyzed or thermally decomposed, they produce $SO_4{}^{-\bullet}$. Once $SO_4{}^{-\bullet}$ are formed, they can react with water (Equation (37)) or with OH^- ions (Equation (38)), resulting in the generation of $^\bullet OH$ [111]. The activation of PMS and PDS/PS by catalysis is shown in Equations (39)–(42). In turn, Equations (43) and (44) show the activation of PDS/PS by Fe^{2+} and Fe^{3+} ions, respectively [112,113].

$$S_2O_8{}^{2-} + hv\text{-heat-}))) \rightarrow 2SO_4{}^{\bullet -} \tag{35}$$

$$HSO_5{}^- + hv\text{-heat-}))) \rightarrow SO_4{}^{\bullet -} + {}^\bullet OH \tag{36}$$

$$SO_4{}^{\bullet -} + H_2O \rightarrow SO_4{}^{2-} + {}^\bullet OH + H^+ \tag{37}$$

$$SO_4{}^{\bullet -} + OH^- \rightarrow SO_4{}^{2-} + {}^\bullet OH \tag{38}$$

$$\text{Semiconductor} + h\nu \rightarrow e^-_{(CB)} + h^+_{(VB)} \tag{39}$$

$$HSO_5^- + e^-_{(CB)} \rightarrow SO_4^{\bullet-} + OH^- \text{ or } SO_4^{2-} + {}^\bullet OH \tag{40}$$

$$S_2O_8^{2-} + e^-_{(CB)} \rightarrow SO_4^{\bullet-} + SO_4^{2-} \tag{41}$$

$$HSO_5^- + h^+_{(VB)} \rightarrow SO_5^{\bullet-} + H^+ \tag{42}$$

$$Fe^{2+} + S_2O_8^{2-} \rightarrow Fe^{3+} + SO_4^{\bullet-} + SO_4^{2-} \tag{43}$$

$$Fe^{3+} + S_2O_8^{2-} + \frac{1}{2}O_2 \rightarrow SO_4^{\bullet-} + Fe^{+2} + SO_4^{2-} + FeO^{2+} \tag{44}$$

Parameters like pH and temperature can influence persulfate-based AOPs. When the solution has an acidic pH, $SO_4^{-\bullet}$ dominate oxidation; and under basic pH, the dominant species are ${}^\bullet OH$. The acidic condition activation of PDS/PS only generates $SO_4^{-\bullet}$; in turn, at basic conditions, $SO_4^{-\bullet}$ react with OH^- ions resulting in the generation of ${}^\bullet OH$ (Equation (38)) [76,112]. Concerning the influence of temperature on the efficiency of the process, a temperature increase can enhance the decomposition of persulfate into $SO_4^{-\bullet}$; meanwhile, when persulfate AOPs are conducted at room temperature, $SO_4^{-\bullet}$ kinetics are slower, decreasing the rate of degradation of organic pollutants [114].

Table 2 lists studies about the treatment of dyes contained in water by using AOPs.
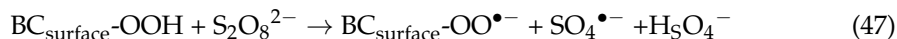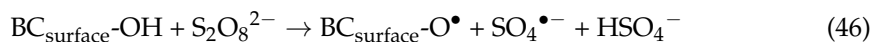
Table 2. Dye treatment by using AOPs.

Advanced Oxidation Process	Dye	Operation Conditions	Results	Ref.
Sono-photocatalysis with ZnO microparticles	Rhodamine B	λ = 554 nm; pH = 5.8; frequency = 59 kHz; [catalyst] = 0.5 g/L; [dye] = 2.5 mg/L	- ~100% removal of the dye - Sono-photocatalysis generates more ${}^\bullet OH$ than sonolysis and photocatalysis alone	[78]
Heterogeneous sono-Fenton with magnetite (Fe_3O_4) nanoparticles	Basic violet 10	pH = 3; [catalyst] = 1.5 g/L; [H_2O_2] = 36 mM; ultrasonic power = 450 W/L; [dye] = 30 mg/L	- 75.94% removal of the dye - ${}^\bullet OH$ were the most abundant radical	[115]
Heterogeneous sono-Fenton like with Fe_3O_4 nanoparticles	Reactive orange 107 (RO107) and real textile wastewater	pH = 5 (simulated water), 8.1 (real textile wastewater); [catalyst] = 0.8 g/L; [H_2O_2] = 10 mM; frequency = 24 kHz	- ~100% removal and 87% mineralization of RO107 - 79.25% removal of COD and 66.54% of total organic carbon (TOC)	[116]
Photo-Fenton	Congo red	pH = 3; λ = 507 nm; [Fe^{2+}] = 10 mg/L; [H_2O_2] = 50 mg/L	- 93% removal of Congo red - 86.54% and 79.9% removal of COD and COT, respectively	[117]
Electro-Fenton	Reactive red 195	pH = 3; [dye] = 50 mg/L; superficial oxygen velocity = 0.012 cm/s; t = 60 min; current density = 2 mA/cm^2	- Color removal efficiency was ≈100% - 96% removal of COD	[118]
Sono-Fenton	Acid violet 7	pH = 3; [Fe^{2+}] = 10 mg/L; [H_2O_2] = 50 mg/L; [dye] = 20 mg/L; frequency = 40 kHz	- COD and dye removal were 81% and ≈100%, respectively - Ultrasonic waves increased ${}^\bullet OH$ production	[119]
Persulfate sono-catalysis with magnetic $CaFe_2O_4$ nanoparticles	Brilliant green (BG)	[Dye] = 50 mg/L; [catalyst] = 0.5 g/L; [persulfate] = 200 mg/L; frequency = 23 kHz; pH = 8.1	- 99.8% removal of BG - $SO_4^{\bullet-}$ and ${}^\bullet OH$ where involved in BG removal	[120]

4.3. Coupling Biochar with AOPs for the Elimination of Dyes in Water

Biochar has gained attention as a heterogeneous catalyst in AOPs due to its chemical-saving synthesis, high dispersion of reactive sites, adjustable physicochemical properties, pore structure and content of oxygen functional groups such as hydroxyl, carboxyl and carbonyl, which can promote the activation of H_2O_2 and persulfate to ${}^\bullet OH$ and $SO_4^{-\bullet}$, respectively, as shown in Equations (45)–(48) [19]. Biochar as a by-product of thermal decomposition of biomass can generate environmentally persistent free radicals [18]. Like oxygen functional groups, environmentally persistent free radicals can activate H_2O_2 and

persulfate; consequently, $^{\bullet}$OH and $SO_4{}^{-\bullet}$ are generated. As expressed in Equations (49) and (50), the catalytic mechanism of environmentally persistent free radicals on biochar surface follows an electron transfer reaction to activate H_2O_2 and persulfate [20]. On the other hand, light plays an important role when biochar is coupled with AOPs since light can activate biochar, inducing the formation of environmental free radicals, $^{\bullet}$OH and singlet oxygen ($^1O_2$) species [18,50,121], leading to an increase in the oxidation potential of the combined system.

It is reported that free radicals are product of the homolytic break up (caused by the thermal decomposition of biomass) of the α- and β-alkyl-aryl ether bonds, carbon–carbon and carbon–oxygen bounds present in lignocellulose; therefore, environmentally persistent free radicals are more abundant in biochar derived from lignocellulose [51]. When electrons are transferred from the phenol and quinone fraction of the biomass to the transition metals, which can be present in biomass or added before the thermochemical decomposition of biomass, this can also form environmentally persistent free radicals [121]. It is important to note that the environmentally persistent free radicals present on the biochar surface can decrease with the increase in temperature when the thermochemical method is used for the decomposition of biomass [122]. The content of environmentally persistent free radicals tends to decrease after the oxidation process, reducing the efficiency of the process. In this regard, the chemical modification of the biochar can overcome this limitation [123].

$$BC_{surface}\text{-}OH + H_2O_2 \rightarrow BC_{surface}\text{-}O^{\bullet} + {}^{\bullet}OH + H_2O \tag{45}$$

$$BC_{surface}\text{-}OH + S_2O_8{}^{2-} \rightarrow BC_{surface}\text{-}O^{\bullet} + SO_4{}^{\bullet-} + HSO_4{}^{-} \tag{46}$$

$$BC_{surface}\text{-}OOH + S_2O_8{}^{2-} \rightarrow BC_{surface}\text{-}OO^{\bullet-} + SO_4{}^{\bullet-} + H_SO_4{}^{-} \tag{47}$$

$$BC_{surface}\text{-}C = O + S_2O_8{}^{2-} \rightarrow BC_{surface}\text{-}CO^{\bullet-} + SO_4{}^{\bullet-} + SO_4{}^{2-} \tag{48}$$

$$H_2O_2 + e^{-} \rightarrow {}^{\bullet}OH + OH^{-} \tag{49}$$

$$HSO_5{}^{-} + e^{-} \rightarrow SO_4{}^{\bullet-} + OH^{-} \text{ or } SO_4{}^{2-} + {}^{\bullet}OH \tag{50}$$

4.4. Biochar Modification

Biochar can be modified by acid and alkaline treatments, heteroatomic doping and metal impregnation [122]. In acid and alkaline treatments, the surface area, porosity and functional groups containing oxygen are improved. With acid treatments, for example, hydroxyl and carboxyl groups are increased, while in alkaline treatments, hydroxyl groups increase on the surface of the biochar [124]. Acid or alkaline modifications consist of a wash of acids or bases like HCl, sulfuric acid (H_2SO_4), phosphoric acid (H_3PO_4), nitric acid (HNO_3), NaOH and potassium hydroxide (KOH). This procedure can be done before or after the biomass thermochemical decomposition [122,125]. Acid and alkaline treatments have several disadvantages. Acid treatments can cause the decrease of biochar surface area and alkaline treatments can cause corrosion to the equipment [19]. Heteroatoms like nitrogen (N), sulfate (S), boron (B) and phosphorus (P) can change biochar electronic structure when it is doped with these atoms [126]. Heteroatom doping is usually performed by adding the heteroatom to the biomass before the mixture is thermo-decomposed, ensuring the distribution of the heteroatom through all the surface of biochar [127]. N doping can enhance the catalytic capacity of biochar for PMS activation by increasing biochar basicity; therefore, the adsorption of PMS on biochar porous and electron transfer reaction between biochar and PMS are promoted [128]. Even though S doping is possible with biochar, research has shown that doping biochar made from rice straw with S has a negative effect on the catalytic ability of biochar. This effect can be ascribed to the substitution of oxygen functional groups by S, causing a reduction in the ability of biochar to activate persulfate or H_2O_2, and decreasing the degradation efficiency of the process [50]. In the case of N, another way to obtain N-doped biochar is by self-doping with N. This method has been described as a simple way to add N to the carbonaceous structure of the biochar maintaining the biochar structure and obtaining a uniform distribution of the N atoms [129]. It is
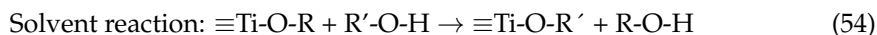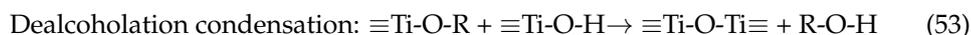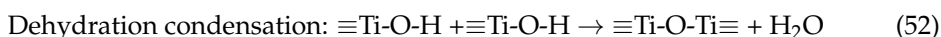
reported that to produce N-doped biochar, biomass containing a high content in proteins is the most indicated type of biomass for this purpose, since this ensures that biochar has high concentrations of N on the surface [130]. Additionally, Binda and coworkers [131] produced a biochar at low temperature from *Nannochloropsis* sp., a marine microalga. The production methodology used allowed for the natural self-doping of the biochar without requiring harsh conditions, providing an efficient strategy for absorbing lead (II) ions in aqueous solution. Lead was also efficiently adsorbed on magnesium oxide embedded N self-doped biochar composites [132].

Metal impregnation of biochar is the modification done in most of the studies where biochar is used as a catalyst in AOPs for the removal of dyes [8,11,21,133–135]. Metal impregnation consists of immersing the biomass or biochar in a solution of metal salt or metal oxide causing the incorporation of metals to the biochar surface or pores [124]. Salts or oxides of metals like Fe, cobalt (Co), manganese (Mn), aluminum (Al), magnesium (Mg) and copper (Cu) have been used for biochar metal impregnation [19,136]. When biochar is modified by metal or metal oxides, there is an improvement in the adsorption efficiency, recyclability and catalytic ability of biochar [41]. For the degradation of methylene blue and methyl orange, Chu et al. [8] used biochar modified with two iron salts (Fe(II) chloride tetrahydrate and Fe(III) chloride hexahydrate) by submerging food waste in a solution containing both iron salts. Afterwards, the mixture was pyrolyzed and the Fe-biochar was used as a heterogeneous catalyst in a sono-Fenton-like process. The Fe-biochar had a synergetic effect in the sono-Fenton-like process by increasing the amount of $^{\bullet}OH$, hence the degradation of the tested dyes was improved [8]. Furthermore, it is reported that the biochar modified by Fe and Mn oxides showed an increase in environmentally persistent radicals; therefore, the degradation efficiency of biochar was increased when it was used in heterogeneous Fenton-like process [137]. In Fenton processes, biochar is mainly used as a supporting material for Fe ions. Therefore, it is used in heterogenous Fenton processes. In this combined process, Fe ions are immobilized on the surface of the biochar, promoting the production of $^{\bullet}OH$ and $SO_4^{-\bullet}$ by the activation of H_2O_2 and persulfate [123].

Metal-based catalysis has the problem of metal leaching, which can cause secondary pollution [51]. Researchers suggest that the use of iron metal composites, like cobalt ferrite ($CoFe_2O_4$), can solve the problem of metal leaching. This does not only solve this problem, but also makes the separation of the biochar simple due to the presence of magnetic metals, such as Fe, and when composites are metals with different valence states the production of ROS is increased due to the redox reactions caused by valence conversion between metals [128].

TiO_2 can be used as a catalyst in the photocatalyst process for the degradation of dyes [138]. To use biochar as a supporter material for TiO_2, the semiconductor must be immobilized on the surface of biochar by wet impregnation and the sol-gel method [139]. Fazal et al. [140] synthesized TiO_2-biochar by wet impregnation. These authors dispersed biochar from macroalgae pyrolysis in isopropanol, followed by an addition of Ti(IV) iso-propoxide. Ultrasound waves were then applied at a frequency of 35 kHz to obtain a uniform mixture, which was heated in a hotplate until evaporation. To remove the solvent content, the TiO_2-biochar was heated in an oven and finally it was calcinated at 400 °C. The TiO_2-biochar used in a heterogeneous photocatalyst process showed higher degradation efficiency for methylene blue than biochar and pure TiO_2 acting individually. The efficiency was increased when associated with a certain amount of dye adsorbed by biochar and the generation of electron holes when TiO_2 supported on biochar reacts with light irradiation (Equation (24)). These electron holes cause the generation of $^{\bullet}OH$ (Equation (25)), which then react with the methylene blue molecules that are adsorbed on biochar surface, causing the degradation of the dye [140]. In turn, the sol-gel method to immobilize TiO_2 on the biochar derived from the pyrolysis of coconut shell was used by Zhang and Lu [141]. These authors started by mixing ethanol and butyl titanate $Ti(C_4H_9O)_4$ by stirring to obtain solution A. For solution B, ethanol (C_2H_5OH), deionized water and acetic acid (CH_3COOH) were mixed with polyethylene glycol ($C_{2n}H_{4n+2}O_{n+1}$). To obtain the sol-gel

solution, solution B was then added dropwise to solution A, aged for 24 h, mixed with the coconut shell biochar, aged again for 24 h and calcinated to obtain the TiO_2-biochar composite. Equations (51)–(55) show the involved reactions ($\equiv$Ti-O-R and R-O-H represent butyl titanate and polyethylene glycol, respectively). The porous nature of the coconut shell biochar favored the formation of TiO_2 in its anatase form. The TiO_2 coconut shell biochar was used as a catalyst in a photocatalytic process in the degradation of brilliant blue KN-R; the biochar favored the contact between TiO_2 and the dye when it was adsorbed in the porous structure of biochar. Additionally, biochar prevented the reaction of e^- and h^+, enhancing the transfer of electron-hole pairs. Thereby, photogenerated h^+ reacted with OH^- on the TiO_2 surface, producing $^\bullet OH$ and favoring the dye degradation [141].

$$\text{Hydrolysis:} \equiv\text{Ti-O-R} + H_2O \rightarrow \equiv\text{Ti-O-H} + \text{R-O-H} \tag{51}$$

$$\text{Dehydration condensation:} \equiv\text{Ti-O-H} + \equiv\text{Ti-O-H} \rightarrow \equiv\text{Ti-O-Ti}\equiv + H_2O \tag{52}$$

$$\text{Dealcoholation condensation:} \equiv\text{Ti-O-R} + \equiv\text{Ti-O-H} \rightarrow \equiv\text{Ti-O-Ti}\equiv + \text{R-O-H} \tag{53}$$

$$\text{Solvent reaction:} \equiv\text{Ti-O-R} + \text{R'-O-H} \rightarrow \equiv\text{Ti-O-R'} + \text{R-O-H} \tag{54}$$

$$\text{Calcination:} \equiv\text{Ti-O-R} \rightarrow \text{O=Ti=O} + H_2O + CO_2 \tag{55}$$

In addition to the use of biochar as a supporter material for TiO_2, biochar has been used as nanoparticles supported on TiO_2 nanotube arrays recently. This type of process has shown a good catalytic activity for the degradation of dyes in water [142]. Furthermore, biochar has been used to modify TiO_2 in order to improve the photocatalytic performance of TiO_2 [143]. Moreover, biochar dots have been utilized to sentitize TiO_2 nanotubes, resulting in the improvement of the photoelectric performance of the process [144].

ZnO-biochar composites have also been used in AOPs for the elimination of dyes in water [145]. ZnO can improve the formation of environmentally persistent free radicals on biochar surface by increasing its catalytic ability [121]. To produce the ZnO-biochar composites, the ball milling method has been reported [139]. This method changes the particle size of the biochar and can modify the functional groups present on the biochar surface [146]. Ball milling is done in a machine where moving balls grind, break and enhance the surface of biochar by a constant mixing and grinding [147]. Yu et al. [16] used the ball milling method to synthesize biochar and ZnO, and used the composite in a photocatalytic process to remove methylene blue in water. Biochar derived from the bamboo stake pyrolysis and ZnO were mixed and ground in agate jars with agate balls. The ZnO addition on the biochar surface enhanced biochar adsorption and catalytic ability; thus, methylene blue removal was increased [16].

Table 3 shows a summary of studies where biochar has been used along with AOPs.

Table 3. Treatment of dyes by coupling biochar with advanced oxidation processes (AOPs).

Process	Dye	Operation Conditions	Results	Reference
Fe-biochar, heterogeneous Fenton process	Amaranth (AM) Sunset yellow (SY)	Biochar: slow pyrolysis, waste coffee grounds, 700 °C, biomass treated with Fe(III) chloride ($FeCl_3$) pH = 3.0; [catalyst] = 0.4 g/L; $[H_2O_2]$ = 5.0 mM; T = 25 °C; t = 60 min	- AM and SY removal of 73.6% and 68%, respectively. AM and SY mineralization of 13.8% and 12.1%, respectively - $^\bullet OH$ causes the cleavage of azo (N=N) functional groups. It dominates the oxidation reaction	[21]
Photocatalyst with ZnO-biochar	Reactive red 97	Biochar preparation: Fast pyrolysis, pecan nutshell, 800 °C, biomass treated with ZnO before pyrolysis pH = 7; t = 67 min	- 100% and 47.10% removal and mineralization of the dye, respectively, with the N=N bonds being broken by $^\bullet OH$ - Zn-biochar shows better efficiency than biochar or ZnO alone	[22]

Table 3. *Cont.*

Process	Dye	Operation Conditions	Results	Reference
Persulfate-AOP with biochar	Reactive brilliant red X-3B	Biochar preparation: pyrolysis, food waste digestate, 800 °C pH = 3.78; [biochar] = 0.5 g/L; [PDS/PS] = 1.5 mM; T = 25 °C; t = 30 min	- 92.21% and 58.32% removal and mineralization, respectively, of the dye $O_2^{\bullet-}$ was the dominant radical, $^{\bullet}OH$, $^1O_2$ and $SO_4^{\bullet-}$ also participated in the oxidation process - Biochar was effective in the activation of PDS/PS	[23]
Fe-biochar heterogeneous Fenton-like process	Rhodamine B	Biochar preparation: slow pyrolysis, sawdust, 600 °C, biochar treated with a Fe^{3+} solution and pyrolyzed at 900 °C pH = 6.5; [biochar] = 2.0 g/L; $[H_2O_2]$ = 4.0 mM; [dye] = 10 mg/L; T = 30 °C	- >92.27% removal of the dye - $^{\bullet}OH$ dominate the oxidation reaction - 58% and 34% reduction of COD and COT, respectively	[133]
Photocatalyst with ZnO-biochar	Methylene blue	Biochar preparation: slow pyrolysis, bamboo stakes, 600 °C, ball milling for ZnO-biochar composite pH = 6.0; [biochar] = 1.0 g/L; [dye] = 160 mg/L; λ = 665 nm; t = 225 min	- 95.19% removal of the dye. Adsorption was the main mechanism due to fast kinetics - ZnO nanoparticles in the biochar surface had a strong photocatalytic activity. Biochar improves the transfer of photo-generated electrons	[16]
MnFe$_2$O$_4$-biochar, heterogeneous Fenton process	Rhodamine B	Biochar preparation: slow pyrolysis, poplar wood flour, 600 °C, biochar treated with a FeCl$_3$, manganese sulfate (MnSO$_4$) and sodium hydroxide (NaOH) solution, and dried to obtain Fe/Mn-biochar pH = 4.8; [biochar] = 0.6 g/L; $[H_2O_2]$ = 115 mM	- 87.6% and 87.9% removal of the dye and TOC, respectively - $O_2^{\bullet-}$ and $^{\bullet}OH$ were the active species in the rhodamine B oxidation - Fe and Mn in the surface of biochar activated H_2O_2 therefore producing $^{\bullet}OH$	[17]
Persulfate-AOP with Mn/Fe-biochar	Orange G	Biochar preparation: slow pyrolysis, sludge, 600 °C, biochar treated with a solution of ferric chloride hexahydrate (FeCl$_3$·6H$_2$O)/Mg(II) chloride (MnCl$_2$·4H$_2$O), pyrolyzed again and treated with ball milling pH = 9; [biochar] = 0.4 g/L; [PMS] = 6 mM; [dye] = 1500 mg/L; T = 25 °C; t = 24 h	- 75.23% removal of the dye - $^{\bullet}OH$ and $SO_4^{\bullet-}$ played a main role - Mn/Fe-biochar composite was efficient in the activation of persulfate - Mn and Fe had a synergetic mechanism, favoring the persulfate activation	[148]
MnFe$_2$O$_4$-biochar, heterogeneous sono-Fenton-like	Methylene blue	Biochar preparation: slow pyrolysis, poplar wood powder, 250 °C, biochar treated with a FeCl$_3$, MnSO$_4$ and NaOH solution, followed by heating pH = 5; [biochar] = 0.7 g/L; $[H_2O_2]$ = 15 mmol/L; [dye] = 20 mg/L; frequency = 20 kHz; T = 25 °C; t = 20 min	- 95% removal of the dye - $^{\bullet}OH$ and $O_2^{\bullet-}$ were the main responsible radicals for the dye treatment - MnFe$_2$O$_4$-biochar composite was efficient in the activation of H_2O_2	[149]
Photocatalyst with TiO$_2$-biochar	Acid orange 7	Biochar preparation: slow pyrolysis, *Salvinia molesta*, 350 °C, biomass pretreated with titanyl sulfate TiOSO$_4$ and titanium isopropoxide (C$_{12}$H$_{28}$O$_4$Ti) [Biochar] = 20 mg/L; λ = 380–480 nm	- 90% removal of the dye - $O_2^{\bullet-}$ and $^{\bullet}OH$ were involved in the oxidation reactions	[150]
Fe-biochar, heterogeneous Fenton	Acid red 1	Biochar preparation: slow pyrolysis, coir pith, 700 °C, biochar treated with a solution of Fe(III) nitrate nonahydrate (Fe(NO$_3$)$_3$·9H$_2$O) and heated again pH = 3; [biochar] = 4 g/L; $[H_2O_2]$ = 16 mM; [dye] = 50 mg/L	- 99.1% and 86.7% removal of acid red 1 and TOC, respectively. - The reaction of Fe^{2+} and H_2O_2 occurred in the surface of biochar, due to the high chemical stability of biochar - Minor leaching of iron	[151]

4.5. Biochar Reusability and Final Disposal

An advantage of using biochar as a catalyst in AOPs is its regeneration ability, which gives it the chance to be used in various cycles [18]. The reusability of biochar when it is used in AOPs makes the catalyst more cost-effective and sustainable [23]. Leichtweis et al. [22] tested the reusability of biochar derived from the pyrolysis of pecan nutshell synthesized with ZnO and used in the degradation of reactive red 97. To recover the biochar composite after each experiment, the ZnO-biochar was washed with deionized water, filtered and dried in an oven at a temperature of 60 °C for 1 h. After 9 cycles, the removal efficiency of ZnO-biochar only decreased by 10% when compared to the first run. The reduction was probably due to the blocking of biochar active sites by intermediates produced in the catalytic reaction, decreasing the available active sites in the ZnO-biochar surface [22].

Liu et al. [23] used biochar derived from the pyrolysis of food digestate as an activator of persulfate in the degradation of reactive brilliant red X-3B and to analyze biochar reusability. The authors tested 3 different regeneration methods: water washing, methanol and re-pyrolysis. After water washing and methanol were used as regeneration methods, biochar was unable to be used again in the activation of persulfate because the carbon structure and functional groups on the biochar surface were damaged during the catalytic reaction; hence, the removal efficiency of the process was seriously decreased. On the other hand, re-pyrolysis of the biochar allows the biochar to be used for 5 cycles more with minimum reduction in its efficiency when compared to the first cycle [23].

Rubeena et al. [151] used iron-doped biochar as a catalyst in a Fenton process for the degradation of acid red 1. To test the Fe-biochar reusability after each cycle, the Fe-biochar was washed with distilled water and dried for 24 h at 80 °C. Fe-biochar was used in 4 cycles; in the first cycle, the removal efficiency of acid red 1 was 96.3% and it decreased to 89.4% in the fourth cycle. The reduction in efficiency was due to blocking of biochar active sites by the intermediate products generated in the catalytic reaction and due to some iron leaching from the biochar surface [151].

Cheng et al. [17], after using $MnFeSO_4$-biochar composite in the degradation of rhodamine B, washed the biochar composite with distilled water prior to drying it at a temperature of 80 °C for 5 h. The biochar $MnFeSO_4$ composites were used in 4 cycles of degradation, showing a minimum decrease even in the fourth cycle (87.8% degradation of rhodamine B). Due to magnetic properties, the biochar was also easy to be removed from the solution, and the leached Fe and Mn ions were present at low concentrations.

Even though biochar used as a catalyst has shown good stability and reusability, its final disposal must be considered [152]. As was described previously, when biochar is used to remove dyes from water, several studies propose the use of disposal methods such as landfill, energy recovery, bio-oil generation or use it as soil fertilizer or soil amendment. However, to the best of the authors' knowledge, there are no studies where biochar is used as a catalyst in AOPs for the removal of dyes evaluating the final disposal of the used catalyst. Taking into consideration that in some cases biochar must be modified with metal ions, metal oxides or metal composites, further efforts must be made to assess the ecotoxicity of the used biochar as a catalyst in the degradation of dyes by AOPs, because not only the dyes on biochar surface could damage the environment and living organisms, but compounds used during the synthesis of the biochar could also represent a risk.

5. Conclusions

From this analysis, biochar can be used to eliminate dyes in water. It can activate H_2O_2 and S_2O_8, generating $^\bullet OH$ and $SO_4^{\bullet-}$, allowing not only for the removal of dyes but also for their degradation. Nonetheless, the ability of biochar to be used as a catalyst can be enhanced by modifying the raw biochar. Therefore, biochar can be used in AOPs like Fenton and other photo-catalytic AOPs. In this regard, the sustainability of the referred processes is further increased. When coupling biochar with AOPs, the removal and degradation rate of dyes rose in comparison with the rates resulting from the use of only biochar. In that way, the dye is not only moved from liquid to solid phase, but it is also degraded into less harmful compounds.

On the other hand, biochar can be regenerated. This ability of biochar gives the opportunity to reduce the operational costs ascribed to wastewater treatments for industries such as the textile industry. Additionally, research shows that it is safe to use the dye-loaded biochar in energy recovery, as soil fertilizer or for soil amendment, as long as the regulatory parameters are met.

Since one of the most claimed capacities of biochar is its sustainability, further studies should be focused on the improvement of the catalytic ability of biochar, reducing the necessity of modifying biochar with metals or other chemicals that can represent an environmental pollution risk. To achieve this purpose, researches should be conducted to

understand more deeply the fundamentals involved in the activation of H_2O_2 and S_2O_8 by biochar.

In this regard, new horizons may be opened by assessing the efficiency of biochar on real wastewater. This constitutes a research challenge in the near future.

References

1. Sirajudheen, P.; Poovathumkuzhi, N.C.; Vigneshwaran, S.; Chelaveettil, B.M.; Meenakshi, S. Applications of chitin and chitosan based biomaterials for the adsorptive removal of textile dyes from water-A comprehensive review. *Carbohydr. Polym.* **2021**, *273*, 118604. [CrossRef] [PubMed]

2. Oyarce, E.; Butter, B.; Santander, P.; Sánchez, J. Polyelectrolytes applied to remove methylene blue and methyl orange dyes from water via polymer-enhanced ultrafiltration. *J. Environ. Chem. Eng.* **2021**, *9*, 106297. [CrossRef]

3. Lei, S.; Wang, S.; Gao, B.; Zhan, Y.; Zhao, Q.; Jin, S.; Song, G.; Lyu, X.; Zhang, Y.; Tang, Y. Ultrathin dodecyl-sulfate-intercalated Mg-Al layered double hydroxide nanosheets with high adsorption capability for dye pollution. *J. Colloid Interface Sci.* **2020**, *577*, 181–190. [CrossRef]

4. Garg, A.; Chopra, L. Dye Waste: A significant environmental hazard. *Mater. Today Proc.* **2021**, *48*, 1310–1315. [CrossRef]

5. Sharma, J.; Sharma, S.; Soni, V. Classification and impact of synthetic textile dyes on Aquatic Flora: A review. *Reg. Stud. Mar. Sci.* **2021**, *45*, 101802. [CrossRef]

6. Rafiq, A.; Ikram, M.; Ali, S.; Niaz, F.; Khan, M.; Khan, Q.; Maqbool, M. Photocatalytic degradation of dyes using semiconductor photocatalysts to clean industrial water pollution. *J. Ind. Eng. Chem.* **2021**, *97*, 111–128. [CrossRef]

7. Kapoor, R.T.; Danish, M.; Singh, R.S.; Rafatullah, M.; HPS, A.K. Exploiting microbial biomass in treating azo dyes contaminated wastewater: Mechanism of degradation and factors affecting microbial efficiency. *J. Water Process Eng.* **2021**, *43*, 102255. [CrossRef]

8. Chu, J.H.; Kang, J.K.; Park, S.J.; Lee, C.G. Application of magnetic biochar derived from food waste in heterogeneous sono-Fenton-like process for removal of organic dyes from aqueous solution. *J. Water Process Eng.* **2020**, *37*, 101455. [CrossRef]

9. Javaid, R.; Qazi, U.Y.; Ikhlaq, A.; Zahid, M.; Alazmi, A. Subcritical and supercritical water oxidation for dye decomposition. *J. Environ. Manag.* **2021**, *290*, 112605. [CrossRef]

10. Çelekli, A.; Al-Nuaimi, A.I.; Bozkurt, H. Adsorption kinetic and isotherms of Reactive Red 120 on Moringa oleifera seed as an eco-friendly process. *J. Mol. Struct.* **2019**, *1195*, 168–178. [CrossRef]

11. Nguyen, D.L.T.; Binh, Q.A.; Nguyen, X.C.; Nguyen, T.T.H.; Vo, Q.N.; Nguyen, T.D.; Tran, T.C.P.; Nguyen, T.A.H.; Kim, S.Y.; Nguyen, T.P.; et al. Metal salt-modified biochars derived from agro-waste for effective congo red dye removal. *Environ. Res.* **2021**, *200*, 111492. [CrossRef] [PubMed]

12. Ahmad, A.; Khan, N.; Giri, B.S.; Chowdhary, P.; Chaturvedi, P. Removal of methylene blue dye using rice husk, cow dung and sludge biochar: Characterization, application, and kinetic studies. *Bioesour. Technol.* **2020**, *306*, 123202. [CrossRef]

13. Chahinez, H.O.; Abdelkader, O.; Leila, Y.; Tran, H.N. One-stage preparation of palm petiole-derived biochar: Characterization and application for adsorption of crystal violet dye in water. *Environ. Technol. Innov.* **2020**, *19*, 100872. [CrossRef]

14. Serrano-Martínez, A.; Mercader-Ros, M.T.; Martínez-Alcalá, I.; Lucas-Abellán, C.; Gabaldón, J.A.; Gómez-López, V.M. Degradation and toxicity evaluation of azo dye Direct red 83:1 by an advanced oxidation process driven by pulsed light. *J. Water Process Eng.* **2020**, *37*, 101530. [CrossRef]

15. Guo, L.; Zhang, K.; Han, X.; Zhao, Q.; Wang, D.; Fu, F.; Liang, Y. Highly efficient visible-light-driven photo-Fenton catalytic performance over $FeOOH/Bi_2WO_6$ composite for organic pollutant degradation. *J. Alloy. Compd.* **2020**, *816*, 152560. [CrossRef]

16. Yu, F.; Tian, F.; Zou, H.; Ye, Z.; Peng, C.; Huang, J.; Zheng, Y.; Zhang, Y.; Yang, Y.; Wei, X.; et al. ZnO/biochar nanocomposites via solvent free ball milling for enhanced adsorption and photocatalytic degradation of methylene blue. *J. Hazard. Mater.* **2021**, *415*, 125511. [CrossRef]

17. Cheng, Z.; Li, S.; Nguyen, T.T.; Gao, X.; Luo, S.; Guo, M. Biochar loaded on $MnFe_2O_4$ as Fenton catalyst for Rhodamine B removal: Characterizations, catalytic performance, process optimization and mechanism. *Colloids Surf. A Physicochem. Eng. Asp.* **2021**, *631*, 127651. [CrossRef]

18. Nidheesh, P.V.; Gopinath, A.; Ranjith, N.; Akre, A.P.; Sreedharan, V.; Kumar, M.S. Potential role of biochar in advanced oxidation processes: A sustainable approach. *Chem. Eng. J.* **2021**, *405*, 126582. [CrossRef]

19. Wang, J.; Cai, J.; Wang, S.; Zhou, X.; Ding, X.; Ali, J.; Zheng, L.; Wang, S.; Yang, L.; Xi, S.; et al. Biochar-based activation of peroxide: Multivariate-controlled performance, modulatory surface reactive sites and tunable oxidative species. *Chem. Eng. J.* **2021**, *428*, 131233. [CrossRef]

20. Huang, D.; Luo, H.; Zhang, C.; Zeng, G.; Lai, C.; Cheng, M.; Wang, R.; Deng, R.; Xue, W.; Gong, X.; et al. Nonnegligible role of biomass types and its compositions on the formation of persistent free radicals in biochar: Insight into the influences on Fenton-like process. *Chem. Eng. J.* **2019**, *361*, 353–363. [CrossRef]

21. Shin, J.; Bae, S.; Chon, K. Fenton oxidation of synthetic food dyes by Fe-embedded coffee biochar catalysts prepared at different pyrolysis temperatures: A mechanism study. *Chem. Eng. J.* **2021**, *421*, 129943. [CrossRef]

22. Leichtweis, J.; Silvestri, S.; Carissimi, E. New composite of pecan nutshells biochar-ZnO for sequential removal of acid red 97 by adsorption and photocatalysis. *Biomass Bioenergy* **2020**, *140*, 105648. [CrossRef]

23. Liu, J.; Huang, S.; Wang, T.; Mei, M.; Chen, S.; Li, J. Peroxydisulfate activation by digestate-derived biochar for azo dye degradation: Mechanism and performance. *Sep. Purif. Technol.* **2021**, *279*, 119687. [CrossRef]

24. Urán-Duque, L.; Saldarriaga-Molina, J.C.; Rubio-Clemente, A. Advanced oxidation processes based on sulfate radicals for wastewater treatment: Research trends. *Water* **2021**, *13*, 2445. [CrossRef]

25. Chen, H.; Yu, X.; Wang, X.; He, Y.; Zhang, C.; Xue, G.; Liu, Z.; Lao, H.; Song, H.; Chen, W.; et al. Dyeing and finishing wastewater treatment in China: State of the art and perspective. *J. Clean. Prod.* **2021**, *326*, 129353. [CrossRef]

26. Diaz-Elsayed, N.; Rezaei, N.; Ndiaye, A.; Zhang, Q. Trends in the environmental and economic sustainability of wastewater-based resource recovery: A review. *J. Clean. Prod.* **2020**, *265*, 121598. [CrossRef]

27. Samsami, S.; Mohamadizaniani, M.; Sarrafzadeh, M.H.; Rene, E.R.; Firoozbahr, M. Recent advances in the treatment of dye-containing wastewater from textile industries: Overview and perspectives. *Process Saf. Environ. Prot.* **2020**, *143*, 138–163. [CrossRef]

28. Murad, H.A.; Ahmad, M.; Bundschuh, J.; Hashimoto, Y.; Zhang, M.; Sarkar, B.; Ok, Y.S. A remediation approach to chromium-contaminated water and soil using engineered biochar derived from peanut shell. *Environ. Res.* **2021**, *204*, 112125. [CrossRef]

29. Liu, M.; Almatrafi, E.; Zhang, Y.; Xu, P.; Song, B.; Zhou, C.; Zeng, G.; Zhu, Y. A critical review of biochar-based materials for the remediation of heavy metal contaminated environment: Applications and practical evaluations. *Sci. Total Environ.* **2021**, *806*, 150531. [CrossRef]

30. Sekar, M.; Mathimani, T.; Alagumalai, A.; Chi, N.T.L.; Duc, P.A.; Bhatia, S.K.; Brindhadevi, K.; Pugazhendhi, A. A review on the pyrolysis of algal biomass for biochar and bio-oil–bottlenecks and scope. *Fuel* **2021**, *283*, 119190. [CrossRef]

31. Li, Y.; Xing, B.; Ding, Y.; Han, X.; Wang, S. A critical review of the production and advanced utilization of biochar via selective pyrolysis of lignocellulosic biomass. *Bioresour. Technol.* **2020**, *312*, 123614. [CrossRef] [PubMed]

32. Elkhalifa, S.; Al-Ansari, T.; Mackey, H.R.; McKay, G. Food waste to biochars through pyrolysis: A review. *Resour. Conserv. Recycl.* **2019**, *144*, 310–320. [CrossRef]

33. Lee, X.J.; Ong, H.C.; Gan, Y.Y.; Chen, W.H.; Mahlia, T.M.I. State of art review on conventional and advanced pyrolysis of macroalgae and microalgae for biochar, bio-oil and bio-syngas production. *Energy Convers. Manag.* **2020**, *210*, 112707. [CrossRef]

34. Gezahegn, S.; Sain, M.; Thomas, S.C. Phytotoxic condensed organic compounds are common in fast but not slow pyrolysis biochars. *Bioresour. Technol. Rep.* **2021**, *13*, 100613. [CrossRef]

35. Yuan, P.; Wang, J.; Pan, Y.; Shen, B.; Wu, C. Review of biochar for the management of contaminated soil: Preparation, application, and prospect. *Sci. Total Environ.* **2019**, *659*, 473–490. [CrossRef]

36. Jeyasubramanian, K.; Thangagiri, B.; Sakthivel, A.; Raja, J.D.; Seenivasan, S.; Vallinayagam, P.; Madhavan, D.; Malathi Devi, S.; Rathika, B. A complete review on biochar: Production, property, multifaceted applications, interaction mechanism and computational approach. *Fuel* **2021**, *292*, 120243. [CrossRef]

37. Gul, E.; Alrawashdeh, K.A.B.; Masek, O.; Skreiberg, Ø.; Corona, A.; Zampilli, M.; Wang, L.; Samaras, P.; Yang, Q.; Zhou, H.; et al. Production and use of biochar from lignin and lignin-rich residues (such as digestate and olive stones) for wastewater treatment. *J. Anal. Appl. Pyrolysis* **2021**, *158*, 105263. [CrossRef]

38. Krysanova, K.; Krylova, A.; Zaichenko, V. Properties of biochar obtained by hydrothermal carbonization and torrefaction of peat. *Fuel* **2019**, *256*, 115929. [CrossRef]

39. Guo, F.; Jia, X.; Liang, S.; Zhou, N.; Chen, P.; Ruan, R. Development of biochar-based nanocatalysts for tar cracking/reforming during biomass pyrolysis and gasification. *Bioresour. Technol.* **2020**, *298*, 122263. [CrossRef]

40. You, S.; Ok, Y.S.; Chen, S.S.; Tsang, D.C.; Kwon, E.E.; Lee, J.; Wang, C.H. A critical review on sustainable biochar system through gasification: Energy and environmental applications. *Bioresour. Technol.* **2017**, *246*, 242–253. [CrossRef]

41. Kumar, A.; Singh, E.; Mishra, R.; Kumar, S. Biochar as environmental armour and its diverse role towards protecting soil, water and air. *Sci. Total Environ.* **2021**, *806*, 150444. [CrossRef]

42. Low, Y.W.; Yee, K.F. A review on lignocellulosic biomass waste into biochar-derived catalyst: Current conversion techniques, sustainable applications and challenges. *Biomass Bioenergy* **2021**, *154*, 106245. [CrossRef]

43. Zhu, X.; Luo, Z.; Diao, R.; Zhu, X. Combining torrefaction pretreatment and co-pyrolysis to upgrade biochar derived from bio-oil distillation residue and walnut shell. *Energy Convers. Manag.* **2019**, *199*, 111970. [CrossRef]

44. Gan, Y.Y.; Ong, H.C.; Show, P.L.; Ling, T.C.; Chen, W.H.; Yu, K.L.; Abdullah, R. Torrefaction of microalgal biochar as potential coal fuel and application as bio-adsorbent. *Energy Convers. Manag.* **2018**, *165*, 152–162. [CrossRef]
45. Sbizzaro, M.; Sampaio, S.C.; dos Reis, R.R.; de Assis Beraldi, F.; Rosa, D.M.; de Freitas Maia, C.M.B.; de Carvalho, C.; do Nascimento, C.T.; da Silva, E.A.; Borba, C.E. Effect of production temperature in biochar properties from bamboo culm and its influences on atrazine adsorption from aqueous systems. *J. Mol. Liq.* **2021**, *343*, 117667. [CrossRef]
46. Wang, S.; Zhang, H.; Huang, H.; Xiao, R.; Li, R.; Zhang, Z. Influence of temperature and residence time on characteristics of biochars derived from agricultural residues: A comprehensive evaluation. *Process Saf. Environ. Prot.* **2020**, *139*, 218–229. [CrossRef]
47. Zhang, M.; Song, G.; Gelardi, D.L.; Huang, L.; Khan, E.; Mašek, O.; Parikh, S.J.; Ok, Y.S. Evaluating biochar and its modifications for the removal of ammonium, nitrate, and phosphate in water. *Water Res.* **2020**, *186*, 116303. [CrossRef]
48. Dai, Y.; Zhang, N.; Xing, C.; Cui, Q.; Sun, Q. The adsorption, regeneration and engineering applications of biochar for removal organic pollutants: A review. *Chemosphere* **2019**, *223*, 12–27. [CrossRef]
49. Dai, L.; Lu, Q.; Zhou, H.; Shen, F.; Liu, Z.; Zhu, W.; Huang, H. Tuning oxygenated functional groups on biochar for water pollution control: A critical review. *J. Hazard. Mater.* **2021**, *420*, 126547. [CrossRef]
50. Zhou, X.; Zhu, Y.; Niu, Q.; Zeng, G.; Lai, C.; Liu, S.; Huang, D.; Qin, L.; Liu, X.; Li, B.; et al. New notion of biochar: A review on the mechanism of biochar applications in advanced oxidation processes. *Chem. Eng. J.* **2021**, *416*, 129027. [CrossRef]
51. Song, G.; Qin, F.; Yu, J.; Tang, L.; Pang, Y.; Zhang, C.; Wang, J.; Deng, L. Tailoring biochar for persulfate-based environmental catalysis: Impact of biomass feedstocks. *J. Hazard. Mater.* **2021**, *424*, 127663. [CrossRef] [PubMed]
52. Barquilha, C.E.; Braga, M.C. Adsorption of organic and inorganic pollutants onto biochars: Challenges, operating conditions, and mechanisms. *Bioresour. Technol. Rep.* **2021**, *15*, 100728. [CrossRef]
53. Khan, N.; Chowdhary, P.; Gnansounou, E.; Chaturvedi, P. Biochar and environmental sustainability: Emerging trends and techno-economic perspectives. *Bioresour. Technol.* **2021**, *332*, 125102. [CrossRef]
54. Yang, X.; Zhu, W.; Song, Y.; Zhuang, H.; Tang, H. Removal of cationic dye BR46 by biochar prepared from *Chrysanthemum morifolium* Ramat straw: A study on adsorption equilibrium, kinetics and isotherm. *J. Mol. Liq.* **2021**, *340*, 116617. [CrossRef]
55. Nnadozie, E.C.; Ajibade, P.A. Isotherm, kinetics, thermodynamics studies and effects of carbonization temperature on adsorption of *Indigo Carmine* (IC) dye using *C. odorata* biochar. *Chem. Data Collect.* **2021**, *33*, 100673. [CrossRef]
56. Rubio-Clemente, A.; Gutiérrez, J.; Henao, H.; Melo, A.M.; Pérez, J.F.; Chica, E. Adsorption capacity of the biochar obtained from *Pinus patula* wood micro-gasification for the treatment of polluted water containing malachite green dye. *J. King Saud Univ. Eng. Sci.* **2021**. In press. [CrossRef]
57. Praveen, S.; Gokulan, R.; Pushpa, T.B.; Jegan, J. Techno-economic feasibility of biochar as biosorbent for basic dye sequestration. *J. Indian Chem. Soc.* **2021**, *98*, 100107. [CrossRef]
58. Gokulan, R.; Avinash, A.; Prabhu, G.G.; Jegan, J. Remediation of remazol dyes by biochar derived from *Caulerpa scalpelliformis*—An eco-friendly approach. *J. Environ. Chem. Eng.* **2019**, *7*, 103297. [CrossRef]
59. Missau, J.; Bertuol, D.A.; Tanabe, E.H. Highly efficient adsorbent for removal of crystal violet dye from aqueous solution by CaAl/LDH supported on biochar. *Appl. Clay Sci.* **2021**, *214*, 106297. [CrossRef]
60. Qiu, B.; Tao, X.; Wang, H.; Li, W.; Ding, X.; Chu, H. Biochar as a low-cost adsorbent for aqueous heavy metal removal: A review. *J. Anal. Appl. Pyrolysis* **2021**, *155*, 105081. [CrossRef]
61. de Farias Silva, C.E.; da Gama, B.M.V.; da Silva Gonçalves, A.H.; Medeiros, J.A.; de Souza Abud, A.K. Basic-dye adsorption in albedo residue: Effect of pH, contact time, temperature, dye concentration, biomass dosage, rotation and ionic strength. *J. King Saud Univ. Eng. Sci.* **2020**, *32*, 351–359.
62. Hanumanthu, J.R.; Ravindiran, G.; Subramanian, R.; Saravanan, P. Optimization of process conditions using RSM and ANFIS for the removal of remazol brilliant orange 3R in a packed bed column. *J. Indian Chem. Soc.* **2021**, *98*, 100086. [CrossRef]
63. Li, X.; Shi, J.; Luo, X. Enhanced adsorption of rhodamine B from water by Fe-N co-modified biochar: Preparation, performance, mechanism and reusability. *Bioresour. Technol.* **2021**, *343*, 126103. [CrossRef]
64. Dai, J.; Meng, X.; Zhang, Y.; Huang, Y. Effects of modification and magnetization of rice straw derived biochar on adsorption of tetracycline from water. *Bioresour. Technol.* **2020**, *311*, 123455. [CrossRef]
65. Choudhary, M.; Kumar, R.; Neogi, S. Activated biochar derived from *Opuntia ficus-indica* for the efficient adsorption of malachite green dye, Cu^{+2} and Ni^{+2} from water. *J. Hazard. Mater.* **2020**, *392*, 122441. [CrossRef] [PubMed]
66. Wu, J.; Yang, J.; Feng, P.; Huang, G.; Xu, C.; Lin, B. High-efficiency removal of dyes from wastewater by fully recycling litchi peel biochar. *Chemosphere* **2020**, *246*, 125734. [CrossRef]
67. Chen, X.L.; Li, F.; Chen, H.; Wang, H.; Li, G. Fe_2O_3/TiO_2 functionalized biochar as a heterogeneous catalyst for dyes degradation in water under Fenton processes. *J. Environ. Chem. Eng.* **2020**, *8*, 103905. [CrossRef]
68. Zazycki, M.A.; Borba, P.A.; Silva, R.N.; Peres, E.C.; Perondi, D.; Collazzo, G.C.; Dotto, G.L. Chitin derived biochar as an alternative adsorbent to treat colored effluents containing methyl violet dye. *Adv. Powder Technol.* **2019**, *30*, 1494–1503. [CrossRef]
69. Gurav, R.; Bhatia, S.K.; Choi, T.R.; Choi, Y.K.; Kim, H.J.; Song, H.S.; Lee, S.M.; Park, S.L.; Lee, H.S.; Koh, J.; et al. Application of macroalgal biomass derived biochar and bioelectrochemical system with Shewanella for the adsorptive removal and biodegradation of toxic azo dye. *Chemosphere* **2021**, *264*, 128539. [CrossRef]
70. Gupta, S.; Sireesha, S.; Sreedhar, I.; Patel, C.M.; Anitha, K.L. Latest trends in heavy metal removal from wastewater by biochar based sorbents. *J. Water Process Eng.* **2020**, *38*, 101561. [CrossRef]

71. Gautam, R.K.; Goswami, M.; Mishra, R.K.; Chaturvedi, P.; Awashthi, M.K.; Singh, R.S.; Giri, B.S.; Pandey, A. Biochar for remediation of agrochemicals and synthetic organic dyes from environmental samples: A review. *Chemosphere* **2021**, *272*, 129917. [CrossRef] [PubMed]

72. Ramrakhiani, L.; Halder, A.; Majumder, A.; Mandal, A.K.; Majumdar, S.; Ghosh, S. Industrial waste derived biosorbent for toxic metal remediation: Mechanism studies and spent biosorbent management. *Chem. Eng. J.* **2017**, *308*, 1048–1064. [CrossRef]

73. Titchou, F.E.; Zazou, H.; Afanga, H.; El Gaayda, J.; Akbour, R.A.; Nidheesh, P.V.; Hamdani, M. Removal of organic pollutants from wastewater by advanced oxidation processes and its combination with membrane processes. *Chem. Eng. Process. Process Intensif.* **2021**, *169*, 108631. [CrossRef]

74. Ma, D.; Yi, H.; Lai, C.; Liu, X.; Huo, X.; An, Z.; Li, L.; Fu, Y.; Li, B.; Zhang, M.; et al. Critical review of advanced oxidation processes in organic wastewater treatment. *Chemosphere* **2021**, *275*, 130104. [CrossRef]

75. Rayaroth, M.P.; Aravindakumar, C.T.; Shah, N.S.; Boczkaj, G. Advanced oxidation processes (AOPs) based wastewater treatment-unexpected nitration side reactions-a serious environmental issue: A review. *Chem. Eng. J.* **2021**, *430*, 133002. [CrossRef]

76. Wang, J.; Wang, S. Reactive species in advanced oxidation processes: Formation, identification and reaction A. *Chem. Eng. J.* **2020**, *401*, 126158. [CrossRef]

77. Ramos, R.O.; Albuquerque, M.V.; Lopes, W.S.; Sousa, J.T.; Leite, V.D. Degradation of indigo carmine by photo-Fenton, Fenton, H_2O_2/UV-C and direct UV-C: Comparison of pathways, products and kinetics. *J. Water Process Eng.* **2020**, *37*, 101535. [CrossRef]

78. Lops, C.; Ancona, A.; Di Cesare, K.; Dumontel, B.; Garino, N.; Canavese, G.; Hérnadez, S.; Cauda, V. Sonophotocatalytic degradation mechanisms of Rhodamine B dye via radicals generation by micro-and nano-particles of ZnO. *Appl. Catal. B Environ.* **2019**, *243*, 629–640. [CrossRef]

79. Anushree, C.; Krishna, D.N.G.; Philip, J. Efficient dye degradation via catalytic persulfate activation using iron oxide-manganese oxide core-shell particle doped with transition metal ions. *J. Mol. Liq.* **2021**, *337*, 116429. [CrossRef]

80. Ramos, M.D.N.; Santana, C.S.; Velloso, C.C.V.; da Silva, A.H.M.; Magalhães, F.; Aguiar, A. A review on the treatment of textile industry effluents through Fenton processes. *Process Saf. Environ. Prot.* **2021**, *155*, 366–386. [CrossRef]

81. Coha, M.; Farinelli, G.; Tiraferri, A.; Minella, M.; Vione, D. Advanced oxidation processes in the removal of organic substances from produced water: Potential, configurations, and research needs. *Chem. Eng. J.* **2021**, *414*, 128668. [CrossRef]

82. Rial, J.B.; Ferreira, M.L. Challenges of dye removal treatments based on IONzymes: Beyond heterogeneous Fenton. *J. Water Process Eng.* **2021**, *41*, 102065. [CrossRef]

83. Ahile, U.J.; Wuana, R.A.; Itodo, A.U.; Sha'Ato, R.; Dantas, R.F. A review on the use of chelating agents as an alternative to promote photo-Fenton at neutral pH: Current trends, knowledge gap and future studies. *Sci. Total Environ.* **2020**, *710*, 134872. [CrossRef] [PubMed]

84. Kurian, M. Advanced oxidation processes and nanomaterials-a review. *Clean. Eng. Technol.* **2021**, *2*, 100090. [CrossRef]

85. Ribeiro, J.P.; Nunes, M.I. RECENT trends and developments in Fenton processes for industrial wastewater treatment–A critical review. *Environ. Res.* **2021**, *197*, 110957. [CrossRef]

86. Zhang, M.H.; Dong, H.; Zhao, L.; Wang, D.X.; Meng, D. A review on Fenton process for organic wastewater treatment based on optimization perspective. *Sci. Total Environ.* **2019**, *670*, 110–121. [CrossRef]

87. Scaria, J.; Gopinath, A.; Nidheesh, P.V. A versatile strategy to eliminate emerging contaminants from the aqueous environment: Heterogeneous Fenton process. *J. Clean. Prod.* **2021**, *278*, 124014. [CrossRef]

88. Lai, C.; Shi, X.; Li, L.; Cheng, M.; Liu, X.; Liu, S.; Li, B.; Yi, H.; Qin, L.; Zhang, M.; et al. Enhancing iron redox cycling for promoting heterogeneous Fenton performance: A review. *Sci. Total Environ.* **2021**, *775*, 145850. [CrossRef]

89. Thomas, N.; Dionysiou, D.D.; Pillai, S.C. Heterogeneous Fenton catalysts: A review of recent advances. *J. Hazard. Mater.* **2021**, *404*, 124082. [CrossRef]

90. Li, Y.; Cheng, H. Chemical kinetic modeling of organic pollutant degradation in Fenton and solar photo-Fenton processes. *J. Taiwan Inst. Chem. Eng.* **2021**, *123*, 175–184. [CrossRef]

91. Oller, I.; Malato, S. Photo-Fenton applied to the removal of pharmaceutical and other pollutants of emerging concern. *Curr. Opin. Green Sustain. Chem.* **2021**, *29*, 100458. [CrossRef]

92. Ismail, S.A.; Ang, W.L.; Mohammad, A.W. Electro-Fenton technology for wastewater treatment: A bibliometric analysis of current research trends, future perspectives and energy consumption analysis. *J. Water Process Eng.* **2021**, *40*, 101952. [CrossRef]

93. Wang, Z.; Liu, M.; Xiao, F.; Postole, G.; Zhao, H.; Zhao, G. Recent advances and trends of heterogeneous electro-Fenton process for wastewater treatment-review. *Chin. Chem. Lett.* **2021**, *33*, 653–662. [CrossRef]

94. Divyapriya, G.; Scaria, J.; Singh, T.A.; Nidheesh, P.V.; Babu, D.S.; Kumar, M.S. Advanced treatment of real wastewater effluents by an electrochemical approach. In *Water Pollution and Remediation: Heavy Metals*; Springer: Cham, Switzerland, 2021; pp. 85–122.

95. Casado, J. Towards industrial implementation of Electro-Fenton and derived technologies for wastewater treatment: A review. *J. Environ. Chem. Eng.* **2019**, *7*, 102823. [CrossRef]

96. de Andrade, F.V.; Augusti, R.; de Lima, G.M. Ultrasound for the remediation of contaminated waters with persistent organic pollutants: A short review. *Ultrason. Sonochem.* **2021**, *78*, 105719. [CrossRef]

97. Camargo-Perea, A.L.; Rubio-Clemente, A.; Peñuela, G.A. Use of ultrasound as an advanced oxidation process for the degradation of emerging pollutants in water. *Water* **2020**, *12*, 1068. [CrossRef]

98. Duan, X.; Zhou, X.; Wang, R.; Wang, S.; Ren, N.Q.; Ho, S.H. Advanced oxidation processes for water disinfection: Features, mechanisms and prospects. *Chem. Eng. J.* **2020**, *409*, 128207.

99. Prakash, L.V.; Gopinath, A.; Gandhimathi, R.; Velmathi, S.; Ramesh, S.T.; Nidheesh, P.V. Ultrasound aided heterogeneous Fenton degradation of Acid Blue 15 over green synthesized magnetite nanoparticles. *Sep. Purif. Technol.* **2021**, *266*, 118230. [CrossRef]

100. Rahmani, A.R.; Mousavi-Tashar, A.; Masoumi, Z.; Azarian, G. Integrated advanced oxidation process, sono-Fenton treatment, for mineralization and volume reduction of activated sludge. *Ecotoxicol. Environ. Saf.* **2019**, *168*, 120–126. [CrossRef]

101. Miklos, D.B.; Remy, C.; Jekel, M.; Linden, K.G.; Drewes, J.E.; Hübner, U. Evaluation of advanced oxidation processes for water and wastewater treatment–A critical review. *Water Res.* **2018**, *139*, 118–131. [CrossRef]

102. Korpe, S.; Rao, P.V. Application of advanced oxidation processes and cavitation techniques for treatment of tannery wastewater-A review. *J. Environ. Chem. Eng.* **2021**, *9*, 105234. [CrossRef]

103. Panda, D.; Manickam, S. Recent advancements in the sonophotocatalysis (SPC) and doped-sonophotocatalysis (DSPC) for the treatment of recalcitrant hazardous organic water pollutants. *Ultrason. Sonochem.* **2017**, *36*, 481–496. [CrossRef]

104. Anandan, S.; Ponnusamy, V.K.; Ashokkumar, M. A review on hybrid techniques for the degradation of organic pollutants in aqueous environment. *Ultrason. Sonochem.* **2020**, *67*, 105130. [CrossRef]

105. Pirsaheb, M.; Moradi, N. A systematic review of the sonophotocatalytic process for the decolorization of dyes in aqueous solution: Synergistic mechanisms, degradation pathways, and process optimization. *J. Water Process Eng.* **2021**, *44*, 102314. [CrossRef]

106. Abdurahman, M.H.; Abdullah, A.Z.; Shoparwe, N.F. A comprehensive review on sonocatalytic, photocatalytic, and sonophoto-catalytic processes for the degradation of antibiotics in water: Synergistic mechanism and degradation pathway. *Chem. Eng. J.* **2021**, *413*, 127412. [CrossRef]

107. Liu, P.; Wu, Z.; Abramova, A.V.; Cravotto, G. Sonochemical processes for the degradation of antibiotics in aqueous solutions: A review. *Ultrason. Sonochem.* **2021**, *74*, 105566. [CrossRef]

108. Leite, C.; Coppola, F.; Monteiro, R.; Russo, T.; Polese, G.; Silva, M.R.; Lourenco, M.; Ferreira, P.; Soares, A.; Pereira, E.; et al. Toxic impacts of rutile titanium dioxide in *Mytilus galloprovincialis* exposed to warming conditions. *Chemosphere* **2020**, *252*, 126563. [CrossRef]

109. Khan, S.H.; Pathak, B. Zinc oxide based photocatalytic degradation of persistent pesticides: A comprehensive review. *Environ. Nanotechnol. Monit. Manag.* **2020**, *13*, 100290. [CrossRef]

110. Ge, L.; Shao, B.; Liang, Q.; Huang, D.; Liu, Z.; He, Q.; Wu, T.; Luo, S.; Pan, Y.; Zhao, C.; et al. Layered double hydroxide based materials applied in persulfate based advanced oxidation processes: Property, mechanism, application and perspectives. *J. Hazard. Mater.* **2021**, *424*, 127612. [CrossRef]

111. Yang, J.; Zhu, M.; Dionysiou, D.D. What is the role of light in persulfate-based advanced oxidation for water treatment? *Water Res.* **2021**, *189*, 116627. [CrossRef]

112. Giannakis, S.; Lin, K.Y.A.; Ghanbari, F. A review of the recent advances on the treatment of industrial wastewaters by Sulfate Radical-based Advanced Oxidation Processes (SR-AOPs). *Chem. Eng. J.* **2021**, *406*, 127083. [CrossRef]

113. Ike, I.A.; Linden, K.G.; Orbell, J.D.; Duke, M. Critical review of the science and sustainability of persulphate advanced oxidation processes. *Chem. Eng. J.* **2018**, *338*, 651–669. [CrossRef]

114. Ushani, U.; Lu, X.; Wang, J.; Zhang, Z.; Dai, J.; Tan, Y.; Wang, S.; Li, W.; Niu, C.; Cai, T.; et al. Sulfate radicals-based advanced oxidation technology in various environmental remediation: A state-of-the–art review. *Chem. Eng. J.* **2020**, *402*, 126232. [CrossRef]

115. Hassani, A.; Karaca, C.; Karaca, S.; Khataee, A.; Açışlı, Ö.; Yılmaz, B. Enhanced removal of basic violet 10 by heterogeneous sono-Fenton process using magnetite nanoparticles. *Ultrason. Sonochem.* **2018**, *42*, 390–402. [CrossRef]

116. Jaafarzadeh, N.; Takdastan, A.; Jorfi, S.; Ghanbari, F.; Ahmadi, M.; Barzegar, G. The performance study on ultrasonic/Fe_3O_4/H_2O_2 for degradation of azo dye and real textile wastewater treatment. *J. Mol. Liq.* **2018**, *256*, 462–470. [CrossRef]

117. Masalvad, S.K.S.; Sakare, P.K. Application of photo Fenton process for treatment of textile Congo-red dye solution. *Mater. Today Proc.* **2021**, *46*, 5291–5297. [CrossRef]

118. Elbatea, A.A.; Nosier, S.A.; Zatout, A.A.; Hassan, I.; Sedahmed, G.H.; Abdel-Aziz, M.H.; El-Naggar, M.A. Removal of reactive red 195 from dyeing wastewater using electro-Fenton process in a cell with oxygen sparged fixed bed electrodes. *J. Water Process Eng.* **2021**, *41*, 102042. [CrossRef]

119. Kodavatiganti, S.; Bhat, A.P.; Gogate, P.R. Intensified degradation of Acid Violet 7 dye using ultrasound combined with hydrogen peroxide, Fenton, and persulfate. *Sep. Purif. Technol.* **2021**, *279*, 119673. [CrossRef]

120. Mukhopadhyay, A.; Tripathy, B.K.; Debnath, A.; Kumar, M. Enhanced persulfate activated sono-catalytic degradation of brilliant green dye by magnetic $CaFe_2O_4$ nanoparticles: Degradation pathway study, assessment of bio-toxicity and cost analysis. *Surf. Interfaces* **2021**, *26*, 101412. [CrossRef]

121. Luo, K.; Pang, Y.; Wang, D.; Li, X.; Wang, L.; Lei, M.; Huang, Q.; Yang, Q. A critical review on the application of biochar in environmental pollution remediation: Role of persistent free radicals (PFRs). *J. Environ. Sci.* **2021**, *108*, 201–216. [CrossRef]

122. Wang, C.; Huang, R.; Sun, R.; Yang, J.; Sillanpää, M. A review on persulfates activation by functional biochar for organic contaminants removal: Synthesis, characterizations, radical determination, and mechanism. *J. Environ. Chem. Eng.* **2021**, *9*, 106267. [CrossRef]

123. Yi, Y.; Luo, J.; Fang, Z. Magnetic biochar derived from *Eichhornia crassipes* for highly efficient Fenton-like degradation of antibiotics: Mechanism and contributions. *J. Environ. Chem. Eng.* **2021**, *9*, 106258. [CrossRef]

124. da Silva Medeiros, D.C.C.; Nzediegwu, C.; Benally, C.; Messele, S.A.; Kwak, J.H.; Naeth, M.A.; Ok, Y.S.; Chang, S.X.; El-Din, M.G. Pristine and engineered biochar for the removal of contaminants co-existing in several types of industrial wastewaters: A critical review. *Sci. Total Environ.* **2021**, *809*, 151120. [CrossRef] [PubMed]

125. Lopes, R.P.; Astruc, D. Biochar as a support for nanocatalysts and other reagents: Recent advances and applications. *Coord. Chem. Rev.* **2021**, *426*, 213585. [CrossRef]

126. Shan, R.; Han, J.; Gu, J.; Yuan, H.; Luo, B.; Chen, Y. A review of recent developments in catalytic applications of biochar-based materials. *Resour. Conserv. Recycl.* **2020**, *162*, 105036. [CrossRef]

127. Gasim, M.F.M.; Lim, J.W.; Low, S.C.; Lin, K.Y.A.; Oh, W.D. Can biochar and hydrochar be used as sustainable catalyst for persulfate activation? *Chemosphere* **2021**, *287*, 132458. [CrossRef]

128. Zhao, C.; Shao, B.; Yan, M.; Liu, Z.; Liang, Q.; He, Q.; Wu, T.; Liu, Y.; Pan, Y.; Huang, J.; et al. Activation of peroxymonosulfate by biochar-based catalysts and applications in the degradation of organic contaminants: A review. *Chem. Eng. J.* **2021**, *416*, 128829. [CrossRef]

129. Duan, X.; O'Donnell, K.; Sun, H.; Wang, Y.; Wang, S. Sulfur and nitrogen co-doped graphene for metal-free catalytic oxidation reactions. *Small* **2015**, *11*, 3036–3044. [CrossRef]

130. Zhang, X.; Tian, J.; Wang, P.; Liu, T.; Ahmad, M.; Zhang, T.; Guo, J.; Xiao, H.; Song, J. Highly-efficient nitrogen self-doped biochar for versatile dyes' removal prepared from soybean cake via a simple dual-templating approach and associated thermodynamics. *J. Clean. Prod.* **2022**, *332*, 130069. [CrossRef]

131. Binda, G.; Faccini, D.; Zava, M.; Pozzi, A.; Dossi, C.; Monticelli, D.; Spanu, D. Exploring the adsorption of Pb on microalgae-derived biochar: A versatile material for environmental remediation and electroanalytical applications. *Chemosensors* **2022**, *10*, 168. [CrossRef]

132. Ling, L.L.; Liu, W.J.; Zhang, S.; Jiang, H. Magnesium oxide embedded nitrogen self-doped biochar composites: Fast and high-efficiency adsorption of heavy metals in an aqueous solution. *Environ. Sci. Technol.* **2017**, *51*, 10081–10089. [CrossRef] [PubMed]

133. Wang, C.; Sun, R.; Huang, R. Highly dispersed iron-doped biochar derived from sawdust for Fenton-like degradation of toxic dyes. *J. Clean. Prod.* **2021**, *297*, 126681. [CrossRef]

134. Lee, J.C.; Kim, H.J.; Kim, H.W.; Lim, H. Iron-impregnated spent coffee ground biochar for enhanced degradation of methylene blue during cold plasma application. *J. Ind. Eng. Chem.* **2021**, *98*, 383–388. [CrossRef]

135. Qiu, Y.; Zhang, Q.; Wang, Z.; Gao, B.; Fan, Z.; Li, M.; Hao, H.; Wei, X.; Zhong, M. Degradation of anthraquinone dye reactive blue 19 using persulfate activated with Fe/Mn modified biochar: Radical/non-radical mechanisms and fixed-bed reactor study. *Sci. Total Environ.* **2021**, *758*, 143584. [CrossRef] [PubMed]

136. Wang, J.; Wang, S. Preparation, modification and environmental application of biochar: A review. *J. Clean. Prod.* **2019**, *227*, 1002–1022. [CrossRef]

137. Li, L.; Lai, C.; Huang, F.; Cheng, M.; Zeng, G.; Huang, D.; Li, B.; Liu, S.; Zhang, M.; Qin, L.; et al. Degradation of naphthalene with magnetic bio-char activate hydrogen peroxide: Synergism of bio-char and Fe–Mn binary oxides. *Water Res.* **2019**, *160*, 238–248. [CrossRef]

138. Sutar, S.; Otari, S.; Jadhav, J. Biochar based photocatalyst for degradation of organic aqueous waste: A review. *Chemosphere* **2021**, *287*, 132200. [CrossRef]

139. Zhao, Y.; Qamar, S.A.; Qamar, M.; Bilal, M.; Iqbal, H.M. Sustainable remediation of hazardous environmental pollutants using biochar-based nanohybrid materials. *J. Environ. Manag.* **2021**, *300*, 113762. [CrossRef]

140. Fazal, T.; Razzaq, A.; Javed, F.; Hafeez, A.; Rashid, N.; Amjad, U.S.; Rehman, M.S.U.; Faisal, A.; Rehman, F. Integrating adsorption and photocatalysis: A cost effective strategy for textile wastewater treatment using hybrid biochar-TiO$_2$ composite. *J. Hazard. Mater.* **2020**, *390*, 121623. [CrossRef]

141. Zhang, S.; Lu, X. Treatment of wastewater containing Reactive Brilliant Blue KN-R using TiO$_2$/BC composite as heterogeneous photocatalyst and adsorbent. *Chemosphere* **2018**, *206*, 777–783. [CrossRef]

142. Pinna, M.; Binda, G.; Altomare, M.; Marelli, M.; Dossi, C.; Monticelli, D.; Spanu, D.; Recchia, S. Biochar nanoparticles over TiO$_2$ nanotube arrays: A green co-catalyst to boost the photocatalytic degradation of organic pollutants. *Catalysts* **2021**, *11*, 1048. [CrossRef]

143. Longfei, Z.; Siqun, W.; Zhilin, C.; Yamei, W. Preparation of wood functional coatings with carbon dots grafted TiO$_2$ for its photocatalytic degradation of formaldehyde gas. *J. Beiging For. Univ.* **2022**, *44*, 113–122.

144. Chen, Q.; Lin, G.; Meng, L.; Zhou, L.; Hu, L.; Nong, J.; Li, Y.; Wang, J.; Yu, Q. Enhanced photoelectric performance of TiO$_2$ nanotubes sensitized with carbon dots derived from bagasse. *Chem. Phys. Lett.* **2020**, *749*, 137428. [CrossRef]

145. Gonçalves, M.G.; da Silva Veiga, P.A.; Fornari, M.R.; Peralta-Zamora, P.; Mangrich, A.S.; Silvestri, S. Relationship of the physicochemical properties of novel ZnO/biochar composites to their efficiencies in the degradation of sulfamethoxazole and methyl orange. *Sci. Total Environ.* **2020**, *748*, 141381. [CrossRef] [PubMed]

146. Zhou, Y.; Qin, S.; Verma, S.; Sar, T.; Sarsaiya, S.; Ravindran, B.; Liu, T.; Sindhu, R.; Patel, A.K.; Binod, P.; et al. Production and beneficial impact of biochar for environmental application: A comprehensive review. *Bioresour. Technol.* **2021**, *337*, 125451. [CrossRef] [PubMed]

147. Amusat, S.O.; Kebede, T.G.; Dube, S.; Nindi, M.M. Ball-milling synthesis of biochar and biochar–based nanocomposites and prospects for removal of emerging contaminants: A review. *J. Water Process. Eng.* **2021**, *41*, 101993. [CrossRef]

148. Hao, H.; Zhang, Q.; Qiu, Y.; Meng, L.; Wei, X.; Sang, W.; Tao, J. Insight into the degradation of Orange G by persulfate activated with biochar modified by iron and manganese oxides: Synergism between Fe and Mn. *J. Water Process Eng.* **2020**, *37*, 101470. [CrossRef]

149. Cheng, Z.; Luo, S.; Li, X.; Zhang, S.; Nguyen, T.T.; Guo, M.; Gao, X. Ultrasound-assisted heterogeneous Fenton-like process for methylene blue removal using magnetic $MnFe_2O_4$/biochar nanocomposite. *Appl. Surf. Sci.* **2021**, *566*, 150654. [CrossRef]

150. Silvestri, S.; Goncalves, M.G.; da Silva Veiga, P.A.; da Silva Matos, T.T.; Peralta-Zamora, P.; Mangrich, A.S. TiO_2 supported on *Salvinia molesta* biochar for heterogeneous photocatalytic degradation of Acid Orange 7 dye. *J. Environ. Chem. Eng.* **2019**, *7*, 102879. [CrossRef]

151. Rubeena, K.K.; Reddy, P.H.P.; Laiju, A.R.; Nidheesh, P.V. Iron impregnated biochars as heterogeneous Fenton catalyst for the degradation of acid red 1 dye. *J. Environ. Manag.* **2018**, *226*, 320–328. [CrossRef]

152. Feng, Z.; Yuan, R.; Wang, F.; Chen, Z.; Zhou, B.; Chen, H. Preparation of magnetic biochar and its application in catalytic degradation of organic pollutants: A review. *Sci. Total Environ.* **2021**, *765*, 142673. [CrossRef] [PubMed]